AEROBIC OXIDATION OF ARABINOSE – GLUCOSE MIXTURES OVER GOLD NANOPARTICLES

Sebastian Franz

Laboratory of Industrial Chemistry and Reaction Engineering
Faculty of Science and Engineering
Åbo Akademi University
Turku, Finland, 2020

ABSTRACT

Sebastian Franz

Aerobic oxidation of arabinose – glucose mixture over gold nanoparticles

This master's thesis was carried out under the supervision of Professor Dmitry Yu. Murzin at the Laboratory of Industrial Chemistry and Reaction Engineering at the Faculty of Science and Engineering, Åbo Akademi University, Finland.

Keywords *Heterogeneous catalysis, alumina support, carbon support, kinetic modelling, aldoses, aldonic acids*

With the recent trend to shift from fossil feedstock to bio-based alternatives for fuels and materials, a range of platform chemicals emerges. Utilization of these platform chemicals is of great importance in the means of biorefining. For this, aldose oxidation has been of interest for several years and the most common, glucose has been intensively studied. However, until now only oxidation of individual sugars has been investigated. This work presents studies on the catalytic oxidation of sugar mixtures of C6 glucose and C5 arabinose and focuses on distinctions in the reaction. Catalysts of sizes ≤65 μm with Au nanoparticle contents of 1 and 2 wt-% supported on Al_2O_3 and various types of carbon-based supports were investigated for oxidation reaction purposes. Compared to other metals, Au exhibits the advantage of bypassing over-oxidation, thus leading to deactivation. TEM revealed a distinct difference in PSD between the supports and a parallel correlation to catalytic activity in oxidation reactions of aldose mixtures. Oxidation reactions of arabinose – glucose mixtures over 1% Au/Al_2O_3 catalysts were performed in a semi-batch reactor under varying conditions using molecular oxygen as the oxidizing agent. The reactions were carried out under controlled pH conditions and at atmospheric pressure. Alkaline pH conditions were applied to enhance reaction rates, yet

notable equilibrium shifts to lactones and fructose were observed at values above pH 8, limiting the pH range. Similarly, temperatures above 70 °C exhibited lower rates and selectivity. Increased partial pressure of oxygen enhanced the rate, though induced losses in selectivity to aldonic acids. Furthermore, investigations on influence of varying arabinose – glucose mass ratios over 1% Au/Al_2O_3 catalyst and influence of catalyst loading were conducted. The catalyst showed low activity during recycling and deactivation is concluded. Finally, a kinetic model representing the catalytic oxidation reactions of arabinose and glucose, respectively, along with the isomerization to fructose and ribulose was developed. The estimated values of the model were concluded to fit well to the experimental data and the model's validity was verified.

ACKNOWLEDGMENTS

I would like to extend my greatest gratitude to Professor Dmitry Yu. Murzin for supervising me in this utterly interesting project combining both analytical methods and reaction engineering associated with heterogeneous catalysis. I would like to thank him for his pedagogic counseling and his patience throughout the project.

Along with Professor Murzin, I would like to thank Professor Tapio Salmi for offering me the opportunity to engage in the project and his advices. Furthermore, I would like to thank Professor Johan Wärnå for his help with the kinetic modelling and Laboratory Manager Dr. Kari Eränen for his practical help in the laboratory.

For the analytical methods of TEM, I would like to thank TEM-operator Laboratory Engineer Markus Peurla (University of Turku, Finland) and Associate Professor Päivi Mäki-Arvela for assistance during the TEM-process. My gratitude also goes to Atte Aho, who helped me with the HPLC equipment.

I would like to thank our collaborators Dr. Irina Simakova (Boreskov Institute of Catalysis, Russia) for providing two of the catalysts supported on alumina and Dr. Nataliya Scherban (L.V. Pisarzhevskiy Institute of Physical Chemistry, Ukraine) for providing the catalysts supported on various types of carbon. I would also like to thank María Herrero, who will continue this work, for assisting me with practical matters.

Finally, I would like to thank the entire collegium of the Laboratory of Industrial Chemistry and Reaction Engineering at Åbo Akademi University for helping me through the complete process and for establishing a cheerful and welcoming working environment, in and outside the laboratory.

Sebastian Franz

Turku, December 2019

ABBREVIATIONS AND NOMENCLATURE

Ara	Arabinose
AraA	Arabinonic acid
C5	Monosaccharide with 5 carbon atoms
C6	Monosaccharide with 6 carbon atoms
Fruc	Fructose
Gluc	Glucose
GlucA	Gluconic acid
GlucurA	Glucuronic acid
MCF	Mesoporous cellular foam
N/A	Not available, not defined
PSD	Particle size distribution
PTFE	Polytetrafluoroethylene
Rib	Ribulose
TEM	Transmission electron microscopy

A	Pre-exponential factor
c_i	Concentration
D_m	Metal dispersion
$\overline{d_p}$	Mean particle diameter
d_p	Particle diameter
E_a	Activation energy
k_i	Rate constant
m_{cat}	Mass of catalyst, catalyst loading
n_i	Reaction order
N^i	Reaction route
pO_2	Partial pressure of oxygen
R	Gas constant (8.31451 $\frac{kJ}{mol\ K}$)
r_i	Reaction rate
S_i	Selectivity
T	Temperature
X_i	Conversion
ρ	Catalyst bulk density

TABLE OF CONTENTS

1 INTRODUCTION

1.1 Biorefining

The principle of biorefining and green chemistry has gained immense popularity over the recent decades. The trend to shift from fossil raw materials to sustainable options has developed into a hot topic in both society and industry and research has strongly focused on this field. However, as a substantial amount of backbone chemicals in our society, making up many of our everyday utilities, is made from fossil-based feedstock, further development is still necessary. Thus, refining of bio-based materials into fuels and materials along with valorization of valuable chemical compounds have become main concepts of biorefining.

Today, biomass is utilized in multiple ways (Fig. 1.1). Besides chemical compounds valorization through pyrolysis, gasification and different fractionation methods biomass is still mostly burnt for energy production purposes. Fractionation of biomass compounds can be done by several different methods and/or a combination of these. Pressurized hot-water extraction (PHWE) is used for valorization of extractives [1], hydrolytic depolymerization and hydrolytic hydrogenation for fractionation of saccharides [2].

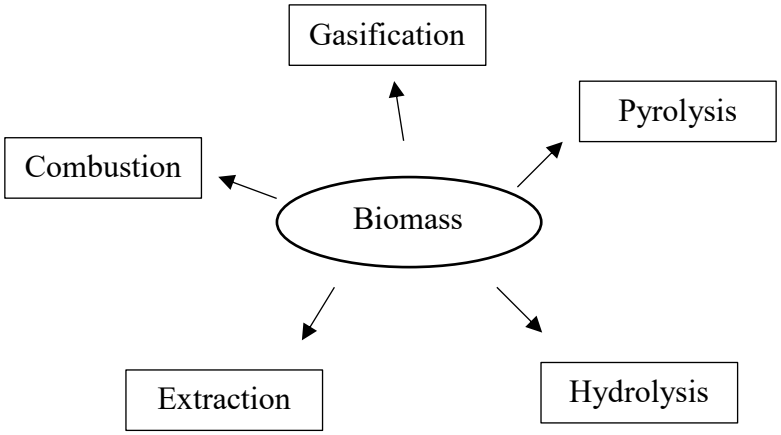

Fig. 1.1. Biomass utilization pathways.

Lignocellulosic biomass, i.e. dry biomass, is split into three major building blocks: cellulose, hemicelluloses and lignin. Lignin serves as the binder in the biomass and is principally present

in the entire biomass. It glues the cells to the fibers together and the fibrils in the cell walls. Lignin consists of heavily branched aromatics connected throughout the plant structure. This results in only one single molecule of lignin in an entire tree, thus making the exact lignin structure difficult to determine

Cellulose is the greatest constituent and is made up from non-branched polysaccharide chains of β-D-glucose. These polymeric saccharides form the cell walls and tissue in biomass and give it the strong structure. Hemicellulose is slightly more complex. It is composed of several different monosaccharide units of pentoses (C6) and hexoses (C5) forming polysaccharides. The backbone can consist of either one or multiple saccharides linked together attached with uniform branching. An example of a hemicellulose are arabinogalactans. The backbone of arabinogalactans consists of β-D-galactose and is branched with β-D-galactose, α-L-arabinose and glucuronic acid side chains [3].

Regarding chemical valorization, obtained aldoses (glucose, arabinose, galactose, etc.) can be considered as platform chemicals for further valorization. Aldose hydrolysis results in an alditol, reaction with an alcohol gives a hemiacetal and acids are formed by oxidation [4]. Gluconic acid, an aldonic acid derived from glucose oxidation, finds its use as a base for buffers or additives in food and beverage products, cosmetics and pharmaceuticals [5].

Extensive research on oxidation of monosaccharides into aldonic, uronic and aldaric acids has been conducted and especially oxidation of glucose has extensively been studied [6-8]. Kusema et al. demonstrated hydrolysis of arabinogalactan in acidic environment and subsequently the individual oxidation of arabinose and galactose monosaccharides [9-11]. Further on, Herrera et al. published a study on simultaneous hydrogenation of monosaccharide mixtures into their respective alcohols [12]. However, so far, no studies on simultaneous oxidation of monosaccharide mixtures into their acids have ever been reported, which confirms the uniqueness of this work.

1.2 Catalysis by gold

To initiate oxidation reactions of aldoses, the presence of a catalyst is essential. Catalysts are defined dependent on their nature and state as either heterogeneous, homogeneous or enzymatic. Studies on the oxidation of glucose to gluconic acid by oxygen have been conducted

by both enzymatically and heterogeneously catalyzed reactions. For oxidation of arabinose to arabinonic acid, reported methods have been conducted with heterogeneous catalysts [10, 13]. Additionally, the storing and handling requirements are less demanding for heterogeneous catalysts, making them a more favorable choice for oxidation reactions of monosaccharide.

Noble metals such as silver, copper, platinum and palladium gained a lot of attention as heterogeneous metal catalysts during the 20th century and are widely used in industry. The awareness of gold (Au) as a catalyst has arisen in the recent decades, especially due to the discovery of the high catalytic activity of small gold particles in low-temperature oxidation of CO [14, 15]. Today, the use of gold as catalysts has besides oxidation reactions been widely extended, including hydrogenation reactions, alkylation reactions and modification reactions of olefins [16]. In oxidation reactions, advantages of gold over other metals is found not only in the catalytic activity, but also in the catalyst stability. When the concentrations of dissolved oxygen exceed the reacting amount of oxygen, oxygen starts to accumulate on the catalyst surface, prohibiting reaction and promoting catalyst deactivation. The deactivation by over-oxidation has been a substantial issue for metal catalysts [17-19]. On the contrary, Tokarev et al., as well as Kusema et al., reported that gold does not encounter over-oxidation and is hence a suitable catalyst for oxidation reactions with oxygen [20, 21]. Fig. 1.2 displays a simple illustration of glucose oxidation with oxygen over a gold catalyst.

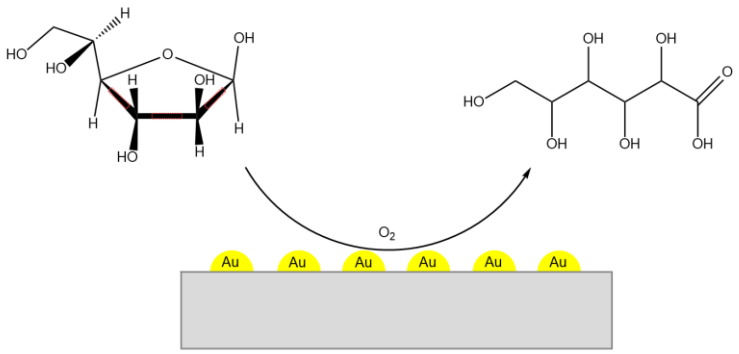

Fig. 1.2. Illustration of oxidation of glucose to gluconic acid by oxygen over supported gold particles.

Various carbon composites, silica and various metal oxides such as CeO_2, TiO_2, Fe_2O_3 and Al_2O_3 have been reported as support materials for Au nanoparticles aimed for oxidation reactions [11, 16, 22]. Carbon has been popular due to its stability in both acidic and alkaline media and the convenient recovery of the catalyst by burning off the carbon [23]. However,

gold catalysts supported on carbon for arabinose oxidation have been reported as less active compared to catalysts supported on Al_2O_3, TiO_2 and ZnO [10]. Although Delidovich et al. presented results for glucose oxidation over Au/C comparable to Au/Al_2O_3 [22], the mean particle sizes of gold nanoparticles supported on carbon are generally significantly larger [21, 24, 25].

1.3 Reaction mechanisms & isomerism

1.3.1 Glucose – Mutarotation & isomerism

In aqueous solutions, D-glucose appears in five different forms (Fig. 1.3-a). Mutarotation conforms the cyclic structure into two anomers, α and β. These anomers of glucose differ in the location of the hydroxyl group of the anomeric center located next to the ether bond. Furthermore, isomerization of the ring gives cyclic hemiacetals of five-membered ring structures (furanose) and six-membered ring structures (pyranose). Each of these four structures, α-D-glucofuranose, β-D-glucofuranose, α-D-glucopyranose and β-D-glucopyranose, is in equilibrium with the acyclic D-glucose form. However, due to the higher strain in the ring of the five-membered structure and thus lower stability, the amount of glucofuranose has been reported to be below 0.2%, while the pyranose form reflects around 99.8% [26]. The acyclic form appears in a very low quantity (0.02%). Noteworthy is that an increased pH favors the formation of the acyclic glucose [13]. The distribution between α-D-glucopyranose and β-D-glucopyranose has been reported to be around 1:2, with 34.2-36% of the α anomer and 64 – 65.8% of the β anomer [27, 28]. However, the trend shows that the amount of furanose increases slightly with temperature [29]. Additionally, in conditions of pH 8 and above, glucose undergoes basic catalyzed isomerization, shifting the carbonyl group from the carbon-1 carbon to the carbon-2, forming fructose (Fig. 1.3-b) [30]. Open-chain aldoses tend to react with the hydroxyl group, being dehydrated into a dehydrogenated aldehydrol form. This intermediate reacts fast with hydrogen to form aldehydrol. For glucose, the ratio between aldehydrol and aldehyde has been reported to be approximately 1:2. Yet, according to the trend, the distribution between aldehydrol and aldehyde favors the hydrated form with a decreased open-chain length [31].

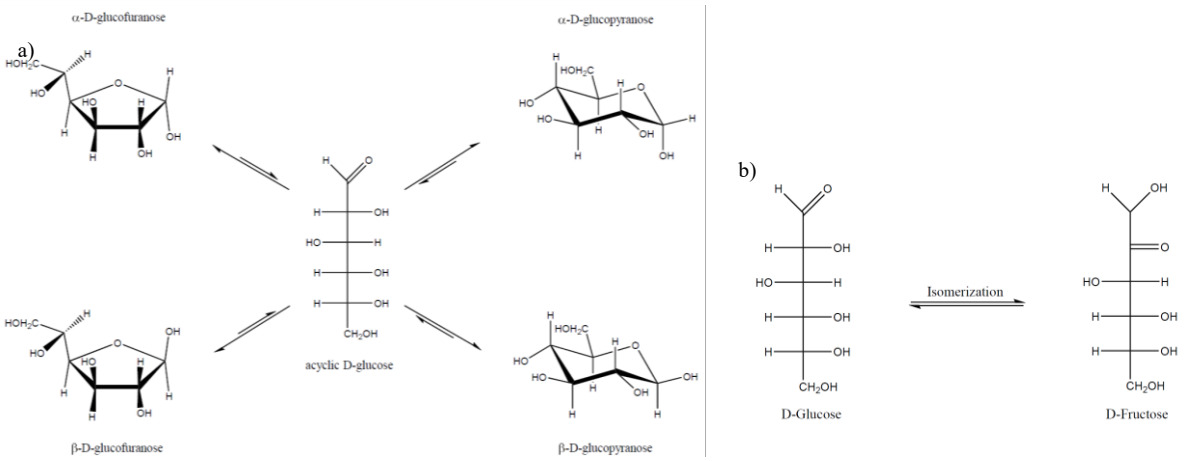

Fig. 1.3. a) Mutarotation of glucose and b) isomerization of glucose into fructose.

1.3.2 Glucose – Reaction mechanism

Following the suggestions for arabinose oxidation presented by Correia et al. [13], two reaction pathways for glucose oxidation are present (Fig. 1.4). In one route, the acyclic glucose is converted into its aldehydrol form after which the molecule is adsorbed onto the catalyst active site. Oxidation results in gluconic acid giving hydrogen peroxide as a by-product. In alkaline conditions, gluconic acid appears as gluconate, as the carboxyl group is deprotonated by the base.

The other route proceeds through the furanose ring form, which adsorbs directly onto the catalyst site. It reacts further to a dehydrated form of glucono-1,4-lactone (glucono-γ-lactone), followed by rapid deprotonation to an ester, isomerization into the more stable six-membered ring of glucono-1,5-lactone (glucono-δ-lactone) and desorption from the catalyst site. Alkaline hydrolysis of the ester group with water opens the lactone ring and results in gluconic acid, which is present as gluconate in alkaline media.

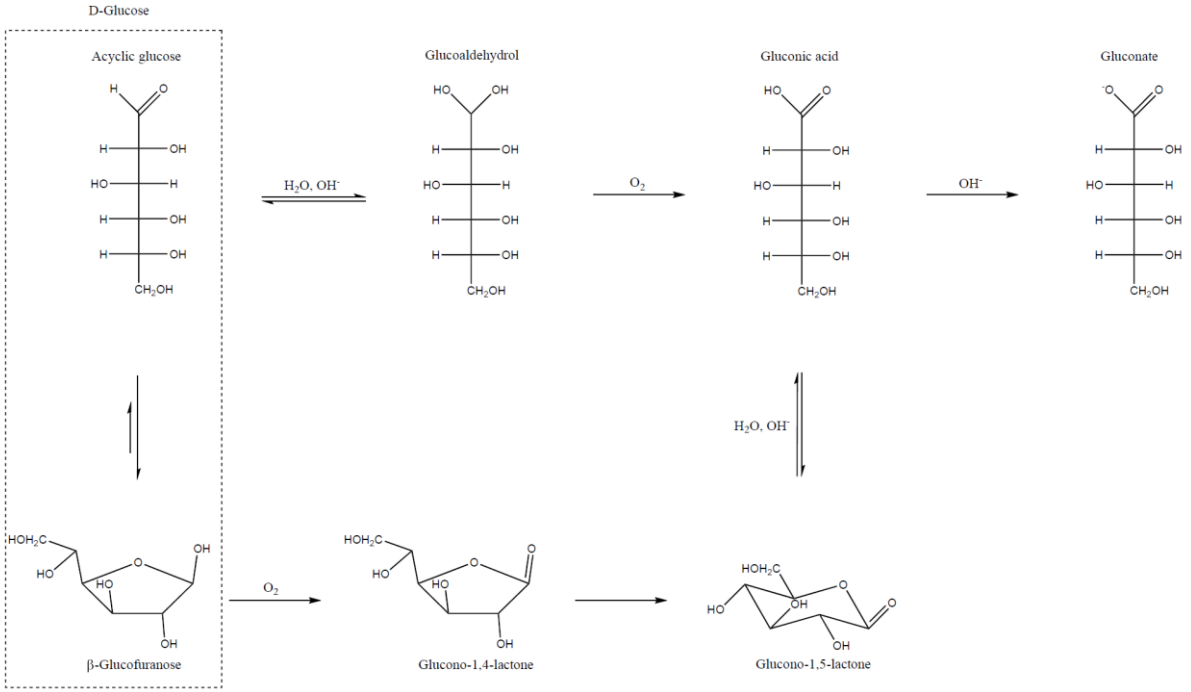

Fig. 1.4. Reaction pathways of D-glucose oxidation.

1.3.3 Arabinose – Mutarotation and isomerism

Similar to glucose, five different conformations of arabinose are present in aqueous solutions; two pyranoses (α, β), two furanoses (α, β) and one acyclic (Fig. 1.5). Since the pyranose form is more stable than the furanose form or the acyclic form, the arabinopyranose form appears as the major component with around 95% (60% α-pyranose, 35% β-pyranose) at 31 °C [29]. The arabinofuranose form represents approximately 4% (3% α-furanose, 1% β-furanose) and the acyclic arabinose the remaining ≤1%. These numbers are notable higher than for glucose at similar conditions.

In most literature, isomerization of arabinose to ribulose is reportedly catalyzed by enzymes [32, 33]. Murzin et al., however, reported aldose – ketose interconversion of arabinose to ribulose over a heterogeneous catalyst at basic pH [34]. Accordingly, the catalytic isomerization of arabinose to ribulose over Au nanoparticles is suggested in this work.

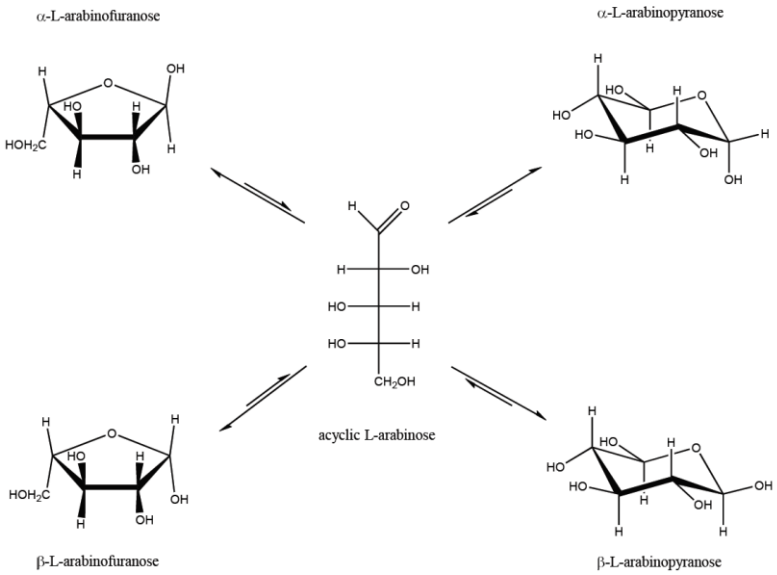

Fig. 1.5. Mutarotation of L-arabinose.

1.3.4 Arabinose – Reaction mechanism

Correia et al. developed a kinetic model for the mechanism of arabinose oxidation where both cyclic and acyclic arabinose are oxidized, following two pathways [13]. Low quantities of both cyclic arabinofuranose and acyclic arabinose indicate their lower stability, allowing to consider both as reactive components. Fig. 1.6 illustrates the reaction pathways for arabinose oxidation.

One reaction route starts from arabinofuranose which is directly adsorbed and oxidized into its arabino-1,4-lactone (arabino-γ-lactone) form and further isomerized into a more stable arabino-1,5-lactone (arabino-δ-lactone). In alkaline aqueous conditions lactone is hydrolyzed and the ring structure is opened. The resulting arabinonic acid is deprotonated in the alkaline media to arabinonate. The other route starts with the acyclic arabinose form, which in alkaline aqueous conditions is transformed into its corresponding aldehydrol form. In this case, the aldehydrol is adsorbed onto the catalyst site and oxidized into arabinonic acid. Again, the acid occurs as arabinonate due to the alkaline conditions.

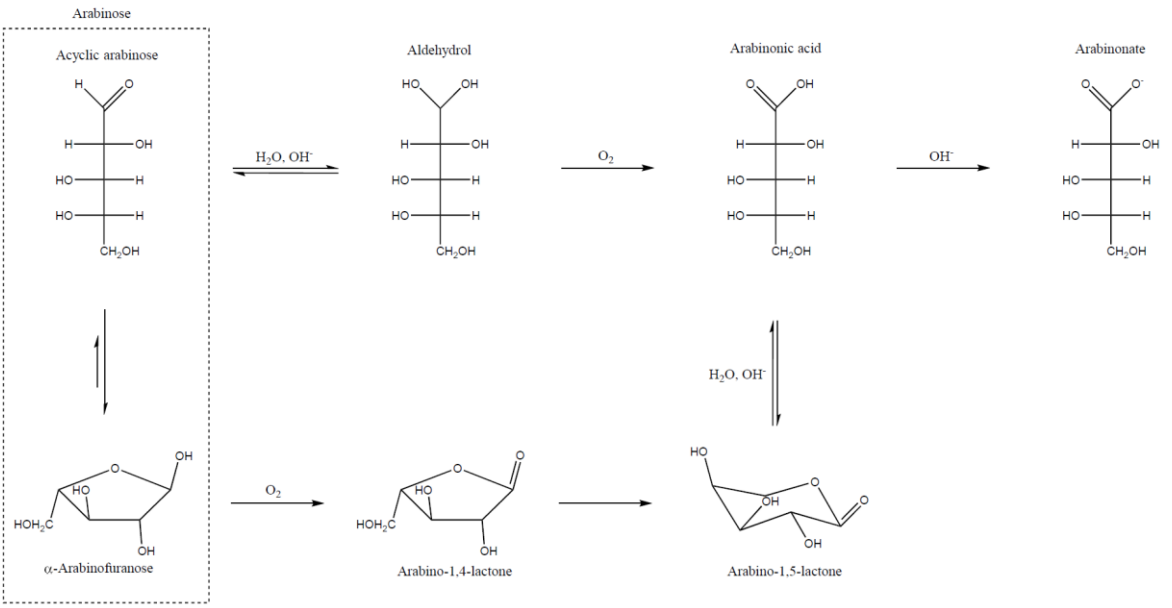

Fig. 1.6. Reaction pathways for L-arabinose oxidation.

1.4 Scope

The objective of this work was to perform catalytic oxidation reactions of sugar mixtures over gold catalysts at constant pH. The reaction was performed in a batch mode reactor and oxygen was used as the oxidizing agent. As catalysts gold nanoparticles supported on different alumina and carbon were used. To investigate and understand the reaction fundamentals, focus was set on the following tasks:

- Screening Au catalysts supported on both Al_2O_3 and different carbon structures in oxidation of sugar mixtures.
- Investigation of a correlation between catalyst particle size and catalytic activity.
- Exploring the influence of such parameters as temperature, pH, oxygen pressure, catalyst mass and sugar ratios.
- Comparison of the individual influence of the parameters on oxidation of C5 arabinose vs C6 glucose.
- Development of a kinetic model based on a feasible reaction mechanism.

2 EXPERIMENTAL

2.1 Catalyst preparation

The support is known to have an influence on the physiochemical and catalytic properties. With the purpose of investigating different supports, catalysts with Au nanoparticles deposited on different types of alumina and carbon were used. Two methods for the preparation of heterogeneous catalyst were selected: direct ion-exchange (DIE) and deposition-precipitation with urea (DPU). In DIE, the metal ions are deposited onto the catalyst surface through electrostatic interactions, while in DPU the reposition relies on supersaturation [35]. The catalysts used in this work were all prepared by different collaborators. In this work, ten different catalysts in the oxidation of glucose and arabinose were studied, as presented in Table 2.1.

Table 2.1. Catalysts used for sugar oxidation.

	Catalyst	Description
a)	1 wt-% Au/Al_2O_3-A	Gold nanoparticles deposited onto alumina.
b)	1 wt-% Au/Al_2O_3-B	Gold nanoparticles deposited onto alumina.
c)	1 wt-% Au/Al_2O_3-C	Gold nanoparticles deposited onto alumina.
d)	2 wt-% Au/C-MCF	Gold nanoparticles deposited onto mesoporous carbon.
e)	2 wt-% Au/C-N-MCF	Gold nanoparticles deposited onto N-doped mesoporous carbon.
f)	2 wt-% Au/C-N-MCF-Ox	Gold nanoparticles deposited onto N-doped mesoporous carbon, higher N content.
g)	2 wt-% Au/C_xN_y-MCF	Gold nanoparticles deposited onto carbon nitride.
h)	2 wt-% Au/C_3N_4	Gold nanoparticles deposited onto graphitic carbon nitride.
i)	2 wt-% Au/C-micro	Gold nanoparticles deposited onto microporous carbon
j)	1 wt-% Au/C	Gold nanoparticles deposited onto active carbon.

2.1.1 Gold nanoparticles on alumina support (Au/Al_2O_3)

Al_2O_3-supported Au catalysts a) and b) (Table 2.1) were prepared by Irina Simakova (Boreskov Institute of Catalysis, Russia) according to the deposition-precipitation method (DPU) presented in [10]. To 1.6 mM aqueous solution of $HAuCl_4$ with urea (0.21 M) heated up to 81 °C, alumina support in powdered form was added. The amount of $HAuCl_4$ solution was calculated to result in the final gold loading of 1% in the catalyst. The suspension of $HAuCl_4$,

urea and Al_2O_3 was mixed under heating at 81 °C for 4 hours and then filtered. Afterwards, the catalysts were washed with water and then additionally with a NH_4OH solution for the removal of excess chloride after deposition of gold onto the support [10, 36]. After further washing with deionized water and filtering, the catalysts were dried at room temperature. Catalyst a) was dried for ca. 6 h and was wet upon the pretreatment, while catalyst b) was dried for 24 and was well dried. Finally, pre-treatment of the catalysts was done in an airflow with an increasing temperature ramp of 2 °C/min until 350 °C.

Catalyst c) (Table 2.1) was prepared by Olga Simakova (Åbo Akademi University) using presumably direct ion exchange analogous to other Al_2O_3-supported catalysts with this Au content [37].

2.1.2 Gold nanoparticles on carbon-based support (Au/C-x)

Carbon-based catalysts (d – i) (Table 2.1) were prepared by Nataliya Scherban (L.V. Pisarzhevskiy Institute of Physical Chemistry, Ukraine). The microporous carbon support i) was prepared by pyrolysis of sucrose. Mesoporous supports d) through f) were carbon-silica composites based on a mesoporous cellular foam (MCF). The composite was obtained by mixing MCF with sucrose and H_2SO_4 in an aqueous solution. Melamine in ethanol was used to functionalize C-N-MCF and C-N-MCF-Ox supports. Removal of silica present as a result from the carbon-silica composites was done by treatment in an aqueous HF solution, washing and drying. Preparation of C_xN_y-MCF was done by pyrolysis of ethylenediamine and CCl_4. C_3N_4 was prepared by the method presented in [38].

The loading of Au onto the catalysts, corresponding to 2 wt-%, was performed according to the procedure described in [39, 40]. After pre-calcination at 150 °C for 2 h, the support (1 g) was mixed with a solution of 25 ml 4.2 mM $HAuCl_4$ and 0.42 M urea and heated under stirring (90 °C, 250 rpm) for 24 h. After cooling, washing and drying, the catalysts were calcined in air at 250 °C for 2 h.

2.2 Catalyst characterization methods

2.2.1 Transmission electron microscopy (TEM)

The particle size was determined using transmission electron microscopy (JEOL JEM-1400Plus). The samples were prepared by suspending the catalyst particles in ethanol and pipetted onto the microscope grid. As highly volatile ethanol evaporated, pure catalyst particles were observed in the imaging. The Au particle size distribution was determined by measuring the particle diameter for over 300 particles for each sample using ImageJ software [41].

2.3 Experimental setup

2.3.1 Reactor setup

All reactions were performed in a 250 ml glass semi-batch slurry reactor (Fig. 2.1). The reactor was equipped with a gas entrainment impeller and a heat jacket using water. The solid catalyst and the liquid were in batch mode, while the gas was continuously fed into the slurry. A Brooks 5850S device was used to control and adjust the gas feed. Excess gas was vented via a heat exchanger to the atmosphere. In this way escape of any vapors, changing the reaction mixture composition, was prevented. Upon entering the reaction mixture, the gas was led through a metal frit to minimize the gas bubble size and, together with efficient agitation, diminishing the limitations by the diffusion of oxygen into the solution. Temperature and pH were controlled with a Metrohm Titrando 907 device equipped with a Metrohm Unitrode electrode.

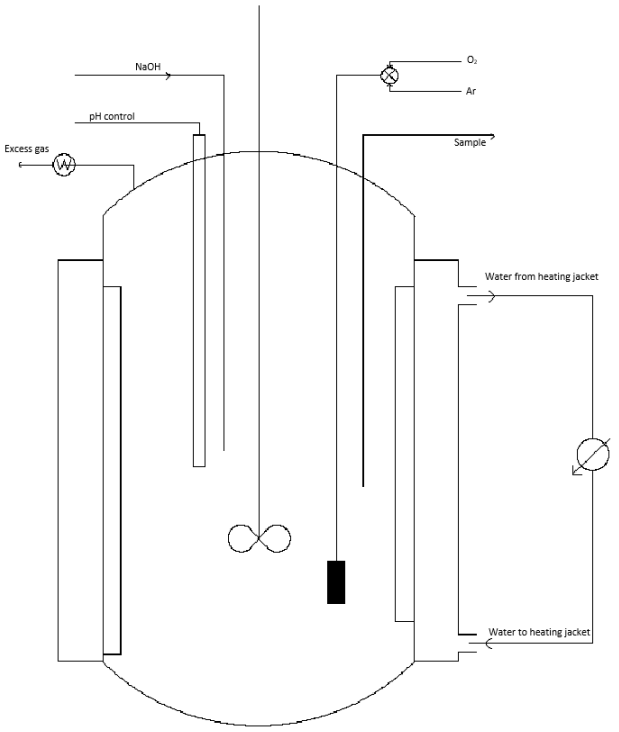

Fig. 2.1. Scheme of reactor setup.

2.3.2 Oxidation of sugars

The reactor was flushed with around 65 ml/min argon and heated to the desired reaction temperature. During flushing, the dry catalyst with particle size < 65 µm was inserted into the reactor. Catalyst particles that remained on the upper reactor walls were washed down to the bottom with 0.5 ml water. Simultaneously, the sugar solution of L-Arabinose (Sigma-Aldrich, ≥99%) and/or anhydrous D-Glucose (Fluka, ≥98%) were heated to approximately 40-50 °C under stirring to minimize the temperature difference. The solution contained in all cases a total amount of 2 g/100ml sugar dissolved in deionized water with a total volume of 150 ml. This specific sugar concentration was chosen as it lies in the same region as the products in the hydrolysis of hemicellulose into monosaccharides, as reported by Kusema et al. [9]. Once the reactor was fully flushed, the sugar solution was poured into the reactor and heated in argon atmosphere to the reaction temperature under stirring and pH control. A high agitation rate of 1000 rpm was used to diminish the influence of external mass transfer limitations. Upon reaching the reaction temperature, the argon flow was reduced to the value used in the reaction and the pre-adjusted oxygen was introduced into the argon flow, resulting in a total gas flow of 40 ml/min. The pH was controlled by addition of 1 M NaOH.

Before taking a sample, a pre-sample of 0.3 ml was withdrawn with a syringe and discarded, after which a fresh sample of 0.7 ml was withdrawn from the reactor. The samples were filtered through a 0.45 µm PVDF filter to avoid catalyst particles from entering the analysis devices and to inhibit further reactions.

2.3.3 Washing of catalysts

For recycling, the catalysts were taken out of the reactor together with the reaction mixture and let to sediment, after which most part of the liquid phase was discarded. The remaining slurry was centrifuged, the liquid removed, the catalyst washed with deionized water and again centrifuged. This process was repeated 3-4 times before the remaining water was dried off. Drying of the catalyst took place in an oven at 58 °C before being stored in a desiccator until reuse.

2.4 Analysis methods

2.4.1 High performance liquid chromatography (HPLC)

Analysis of the reactants and products was performed by high performance liquid chromatography (VWR Hitachi Chromaster) equipped with a 300x7.8 mm Bio-Rad Aminex HPX-87C column and a RI detector (VWR Hitachi Chromaster 5450). The operating temperature of the column was set to 80 °C and the flow rate 0.6 ml/min using 1.2 mM $CaSO_4$ as the eluent, resulting in a column backpressure ranging between 65 and 70 bar. The injection volume of the sample was set to 10 µl.

Identification of the products was done by comparing the retention time with the standards as well as by applying the splicing method (Table 2.2). Quantification was performed by calibrating a series of samples of known concentrations. The slope from the linear plot of the concentration as a function of the peak area, was used to determine the concentrations.

It should be mentioned that the peaks of glucono-δ-lactone and gluconic acid overlap. Hence, the glucono-δ-lactone was neglected and instead counted into the gluconic acid. The remaining data concerning calibration are available in Appendix I.

Table 2.2: Retention times of calibrated reactants and products.

Component	HPLC-RI, V=0.6 ml/min [min]	HPLC-RI, V=0.3 ml/min [min]
Glucose	10.6	21.1 – 21.9
Fructose	13.8 – 13.9	27.5 – 27.6
Gluconic acid	22.1 – 24.9	43.2 – 48.2
Glucuronic acid	8.7 – 9.6	17.2 – 17.7
Glucono-δ-lactone	N/A	43.3 – 44.4
Arabinose	13.8 – 13.9	27.5 – 27.7
Arabinonic acid	16.1 – 18.0	33.2 – 36.3
Arabino-γ-lactone	11.3 – 11.4	22.6 – 23.3
Ribulose	22.5 – 22.6	N/A

2.4.2 Inductively coupled plasma mass spectrometry (ICP-MS)

Potential leaching of metal particles into the liquid phase during the reaction was investigated by inductively coupled plasma mass spectrometry (PerkinElmer, Elan 6100 DRC Plus). The liquid samples, placed in a PTFE vessel, were dissolved in aqua regia solution in a microwave oven (Anton Paar, Multiwave 3000). Subsequently, the samples were diluted with water, first to 100 ml and then further to volumetric ratio 1:5. The acids used for the aqua regia solution were of Suprapur® grade (30% HCl, Merck; 65% HNO3, Merck). For calibration, a commercial multielement standard was used.

3 RESULTS AND DISCUSSION

3.1 Catalyst characterization

Catalyst characterization was carried out by transmission electron microscopy (TEM) for determination of the particle size distribution (PSD) of gold on the catalyst support. Reportedly, catalytic oxidation of sugars is structure sensitive with a maximum catalyst activity at cluster size 2.3 nm, exponentially decreasing at higher and lower sizes [37]. Large particle sizes (d_p) for the carbon-based catalysts were hypothesized and thus only two carbon-based catalysts (see Section 3.2.1) were investigated along with all three Al_2O_3-supported catalysts (Fig. 3.1-Fig. 3.5).

The PSD was determined by manually measuring d_p for over 300 Au particles from at least six different positions, which also was used for calculating the mean particle size ($\overline{d_p}$) from equation (1). However, particles of sizes larger than 10 nm were not considered, as they were presumably not affecting the oxidation reaction. Therefore, also the calculation of the turnover frequency was pretermitted.

$$\overline{d_p} = \frac{\sum_{i=1}^{N} d_{p,i}}{N} \quad , d_{p,i} \leq 10\ nm \tag{1}$$

Table 3.1 lists the catalysts analyzed by TEM together with their corresponding $\overline{d_p}$. Throughout the work, the catalyst percentage values indicate weight percentage.

Table 3.1. Mean particle diameter $\overline{d_p}$ and the particle size at the peak of the Gaussian fit $d_{p,Gauss}$.

Catalyst		$\overline{d_p}$ [nm]	D_m [%]	$d_{p,Gauss}$
a)	1% Au/Al_2O_3-A	2.83	35.34	2.71
b)	1% Au/Al_2O_3-B	2.63	38.02	2.16
c)	1% Au/Al_2O_3-C	2.82	35.46	1.57
d)	2% Au/C-MCF	3.85	25.97	1.95
e)	2% Au/C-N-MCF	N/A	N/A	N/A
f)	2% Au/C-N-MCF-Ox	N/A	N/A	N/A
g)	2% Au/C_xN_y-MCF	N/A	N/A	N/A
h)	2% Au/C_3N_4	N/A	N/A	N/A
i)	2% Au/C-micro	N/A	N/A	N/A
j)	1% Au/C	4.65	21.51	4.25

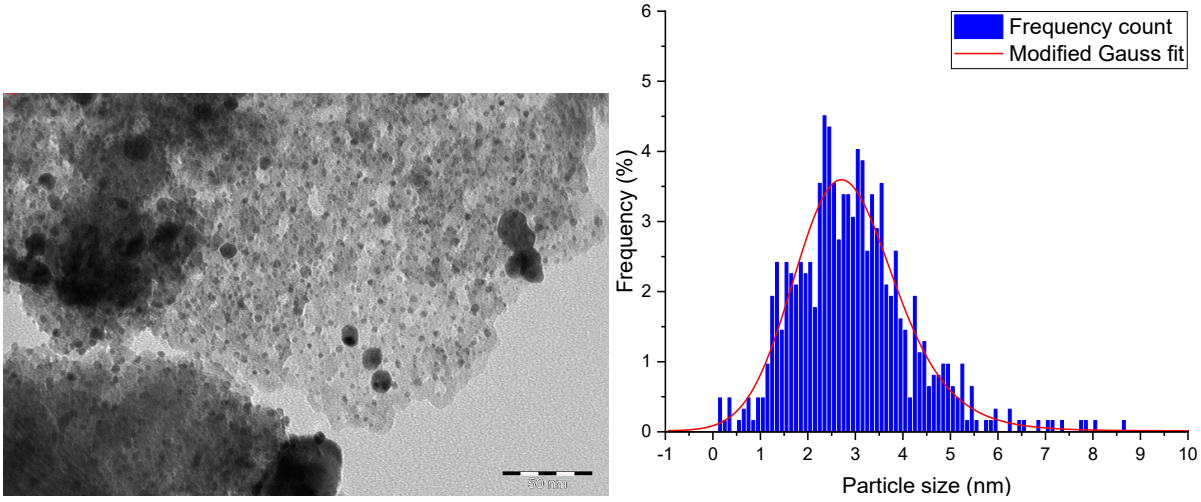

Fig. 3.1. TEM image and PSD of 1% Au/Al_2O_3-A for $d_p \leq 10$ nm.

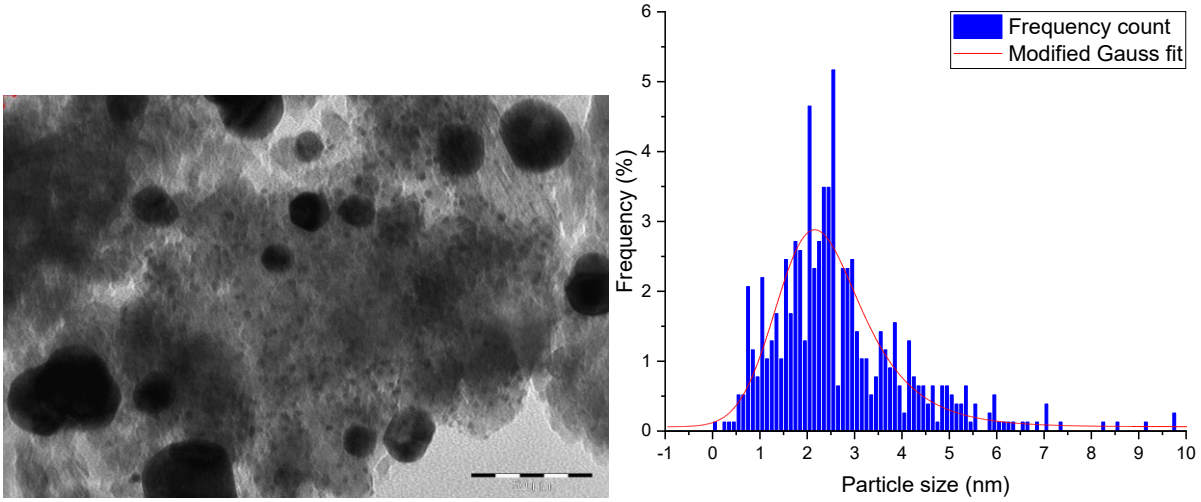

Fig. 3.2. TEM image and PSD of 1% Au/Al_2O_3-B for $d_p \leq 10$ nm.

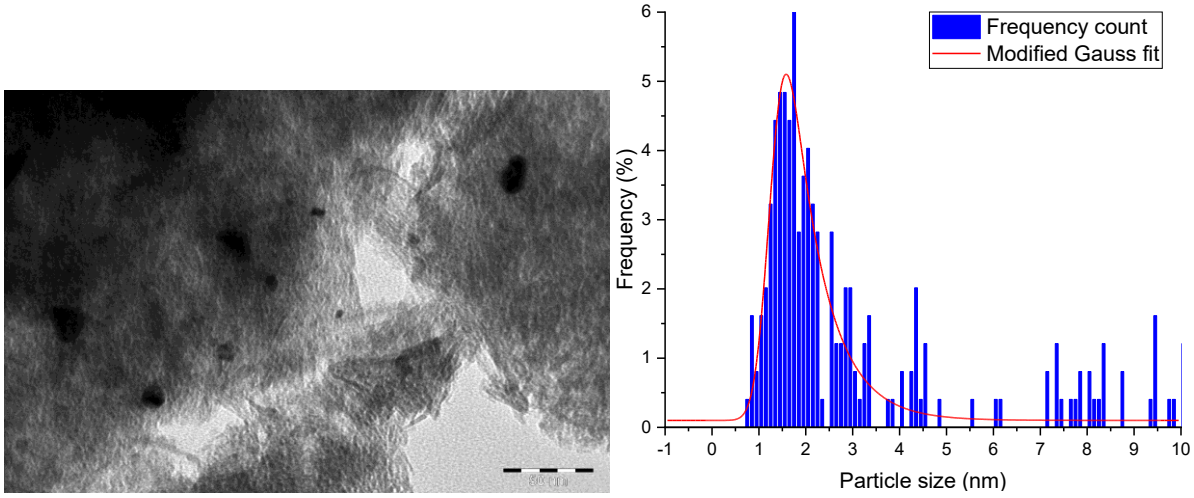

Fig. 3.3. TEM image and PSD of 1% Au/Al_2O_3-C for $d_p \leq 10$ nm.

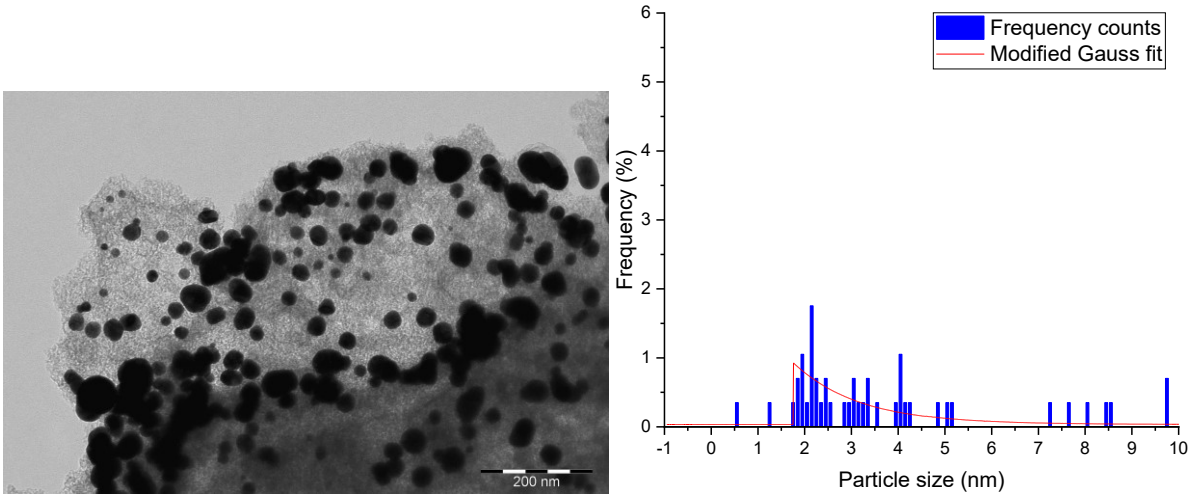

Fig. 3.4. TEM image and PSD of 2% Au/C-MCF for $d_p \leq 10$ nm.

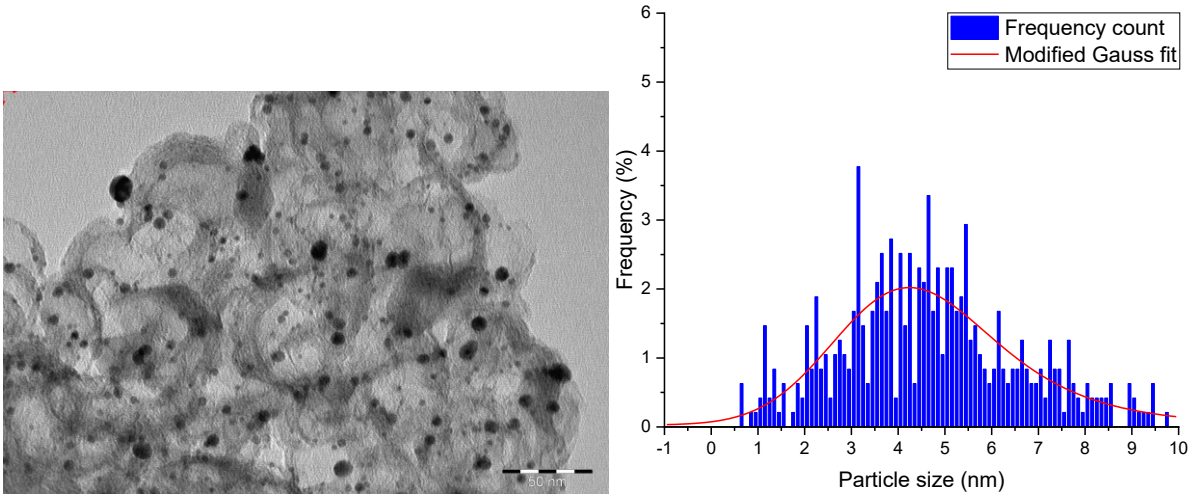

Fig. 3.5. TEM image and PSD of 1% Au/C for $d_p \leq 10$ nm.

Au catalysts supported on Al_2O_3 demonstrated a PSD certainly closer to the reported optimum than carbon-supported catalysts. The largest difference between Al_2O_3-supported catalysts was the percentage of particles of size below ≤10 nm. For catalyst 1% Au/Al_2O_3-B particles sizes of up to 77 nm were observed while for the other Al_2O_3-supported catalysts all particles were ≤35 nm. Due to the large interval, catalyst 1% Au/Al_2O_3-B had only 75% of the counted particles within the interval of below 10 nm, while 1% Au/Al_2O_3-A and 1% Au/Al_2O_3-C had 85% and 99%, respectively. On the other hand, application of a modified Gauss fit, implemented in the Origin software, for particles ≤10 nm showed that catalyst 1% Au/Al_2O_3-B peaked at around $d_{p,Gauss} = 2.2$ nm. This implies that most of the counted particles are around this size. Compared to the other catalysts, this is the closest to the reported optimal particle size.

For catalyst 2% Au/C-MCF only 15% of the counted particles were within the 10 nm interval. For these particles, $\overline{d_p}$ was calculated to 3.85 nm. Simultaneously, particles with sizes up to 138 nm were measured, resulting in an exceedingly broad overall PSD. In comparison, catalyst 1% Au/C had 93% of the particles within this area. $\overline{d_p}$, however, was significantly larger with 4.65 nm for particles ≤ 10 nm. The modified Gaussian distribution fit peaked at 1.95 and 4.25 nm for catalysts 2% Au/C-MCF and 1% Au/C, respectively. For catalyst 2% Au/C-MCF, however, should be considered with care due to a low amount of particles ≤ 10 nm. Graphs for the full PSD range are available in Appendix II.

Catalyst 1% Au/Al_2O_3-B was also analyzed after an oxidation reaction of 1:1 arabinose – glucose mixture at 70 °C, pH 8 and 0.125 atm pO_2. Prior to imaging, the catalyst was washed according to the method described in Section 2.3.3. Larger particles were not to be found in the same quantity as for the fresh catalyst. Comparison of measured PSD (Fig. 3.6) between the fresh and the used catalyst confirmed these observations. Based on these observations an ICP-MS analysis was conducted (see Section 3.2.7).

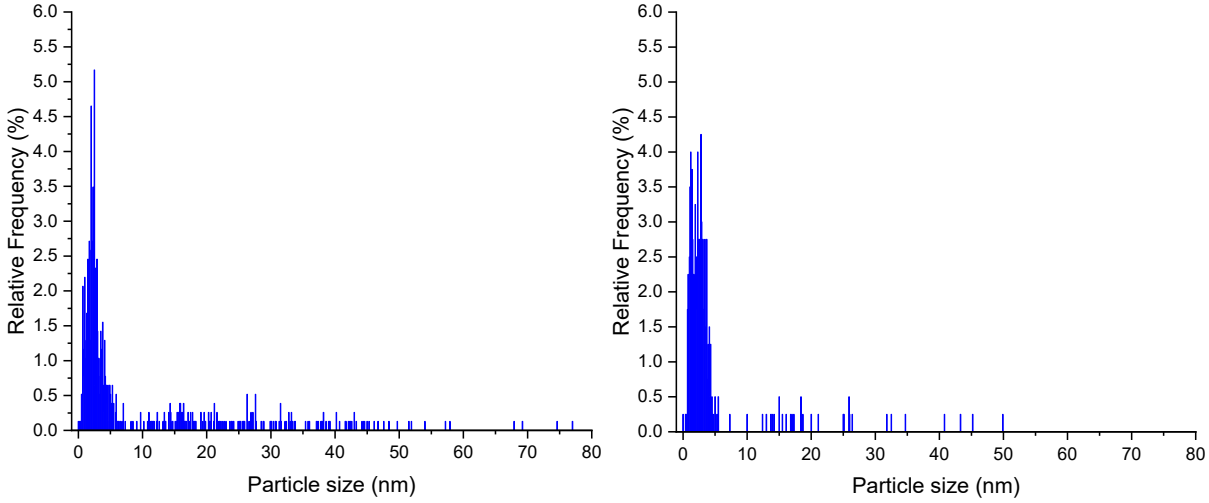

Fig. 3.6. PSD of fresh (left) and used (right) 1% Au/Al_2O_3-B catalyst.

For Al_2O_3-supported catalysts, fiber-like structures were observed (Fig. 3.7-i – iii). These structures consist of pseudoboehmite, AlOOH, a precursor for γ-Al_2O_3 formation by calcination [42]. However, a correlation between the particle size and pseudoboehmite structures was not observed. Silica particles remaining from the catalyst preparation were observed for Au/C-MCF (Fig. 3.7-iv).

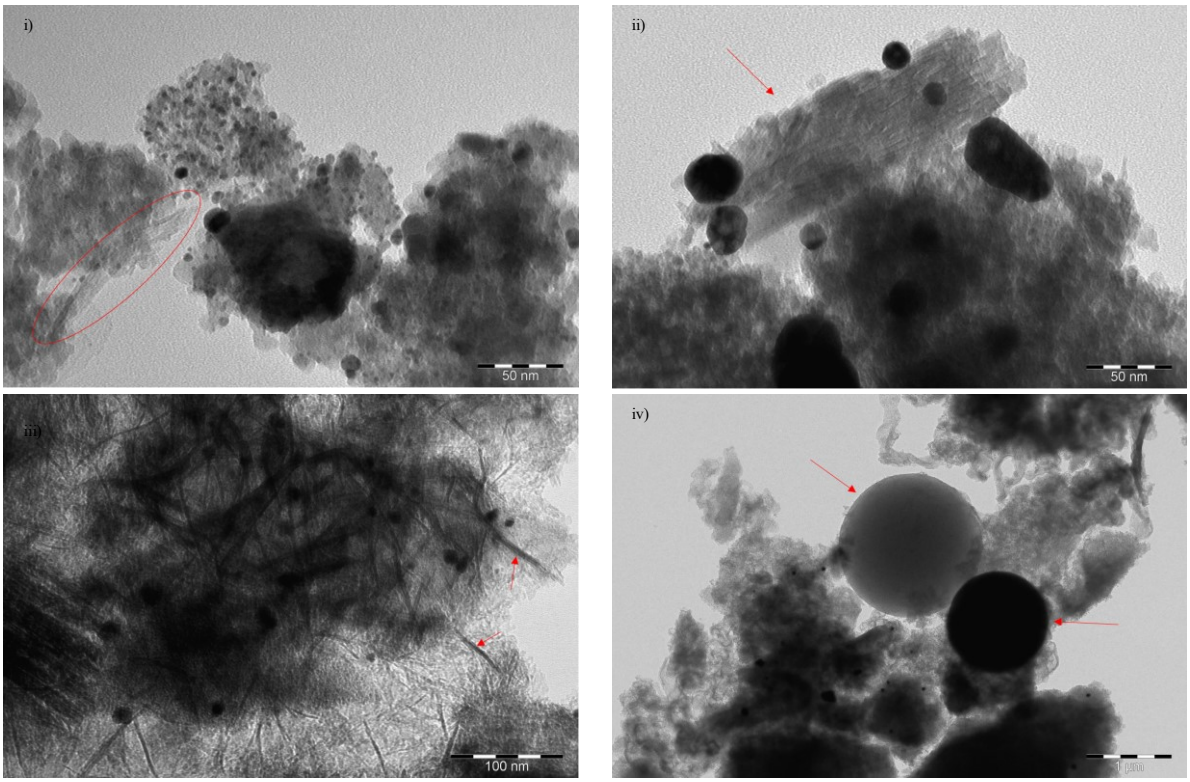

Fig. 3.7. i), ii) and iii): pseudoboehmite structures of Al_2O_3-supported catalysts 1% Au/Al_2O_3-A, 1% Au/Al_2O_3-B and 1% Au/Al_2O_3-C, respectively. iv): Si-shaped impurities in 2% Au/C-MCF catalyst.

3.2 Oxidation of sugars

During oxidation of sugars, a special focus was put on six parameters which were suspected to influence the reaction. Catalyst support, temperature, pH, mass of catalyst, sugar concentrations and partial pressure of oxygen were the key issues studied. The reaction with 1% Au/Al_2O_3-B and conditions of 1:1 arabinose – glucose mass ratio, 70 °C, pH 8, pO_2 = 0.125 atm and m_{cat} = 0.1 g was used as a reference reaction. The use of mass ratios is justified by the compatibility to the industrial use of units. In this work, the converted values of mass ratios to molar ratios are presented in Table 3.3. The stirring speed of 1000 rpm was constant for all experiments. The pH control setup ensured minimal pH fluctuations of ±0.1 from the set point. It has been verified that under similar conditions, the external mass transfer limitations can be neglected [21]. Due to the small catalyst particle size, internal mass transfer limitations were also neglected.

Noteworthy are issues with the reaction setup which appear upon reaction start. When the solution is poured into the reaction and flushed with argon, the liquid contains oxygen but is not saturated. Consequently, the initial reaction rate was thus influenced by oxygen saturation.

3.2.1 Catalyst support screening

In total ten gold catalysts supported on either carbon, carbon composites or alumina were investigated (Table 3.2). Oxidation reactions were carried out at 70 °C, pH 8 and pO_2 = 0.125 atm with 1:1 arabinose – glucose mass ratio. Due to the limited amounts of the catalysts, the catalyst loadings fluctuates between the reactions.

Table 3.2. Mass of catalyst used in oxidation reactions for catalyst support screening purposes.

Catalyst		m_{cat}
a)	1% Au/Al_2O_3-A	0.20
b)	1% Au/Al_2O_3-B	0.10
c)	1% Au/Al_2O_3-C	0.25
d)	2% Au/C-MCF	0.25
e)	2% Au/C-N-MCF	0.20
f)	2% Au/C-N-MCF-Ox	0.23
g)	2% Au/C_xN_y-MCF	0.25
h)	2% Au/C_3N_4	0.20
i)	2% Au/C-micro	0.18
j)	1% Au/C	0.20

The results displayed significant differences in catalytic activities between the catalysts (Fig. 3.8 & Fig. 3.9). Catalysts with carbon-based supports showed low to negligible catalytic activity compared to Al_2O_3-supported catalysts. From Table 3.2, catalysts f), h), i) and j) showed minor or no catalytic activity. For catalyst h) a significant formation of fructose could be suggested, as the amount of arabinose appeared to increase while the amount of glucose decreased and no aldonic acids were formed. Since the peaks of arabinose and fructose overlap, glucose isomerization to fructose was hypothesized. The appearance of fructose is also determined for catalyst e), where fructose formation contributes to convergence of the mass balance closure. The carbon-supported catalysts that exhibit significant acid formation, i.e. catalysts d), e) and g) show besides arabinonic acid an equal selectivity to both gluconic and glucuronic acid. For Al_2O_3-supported catalysts, glucuronic acid was either not observed or present in negligible amounts.

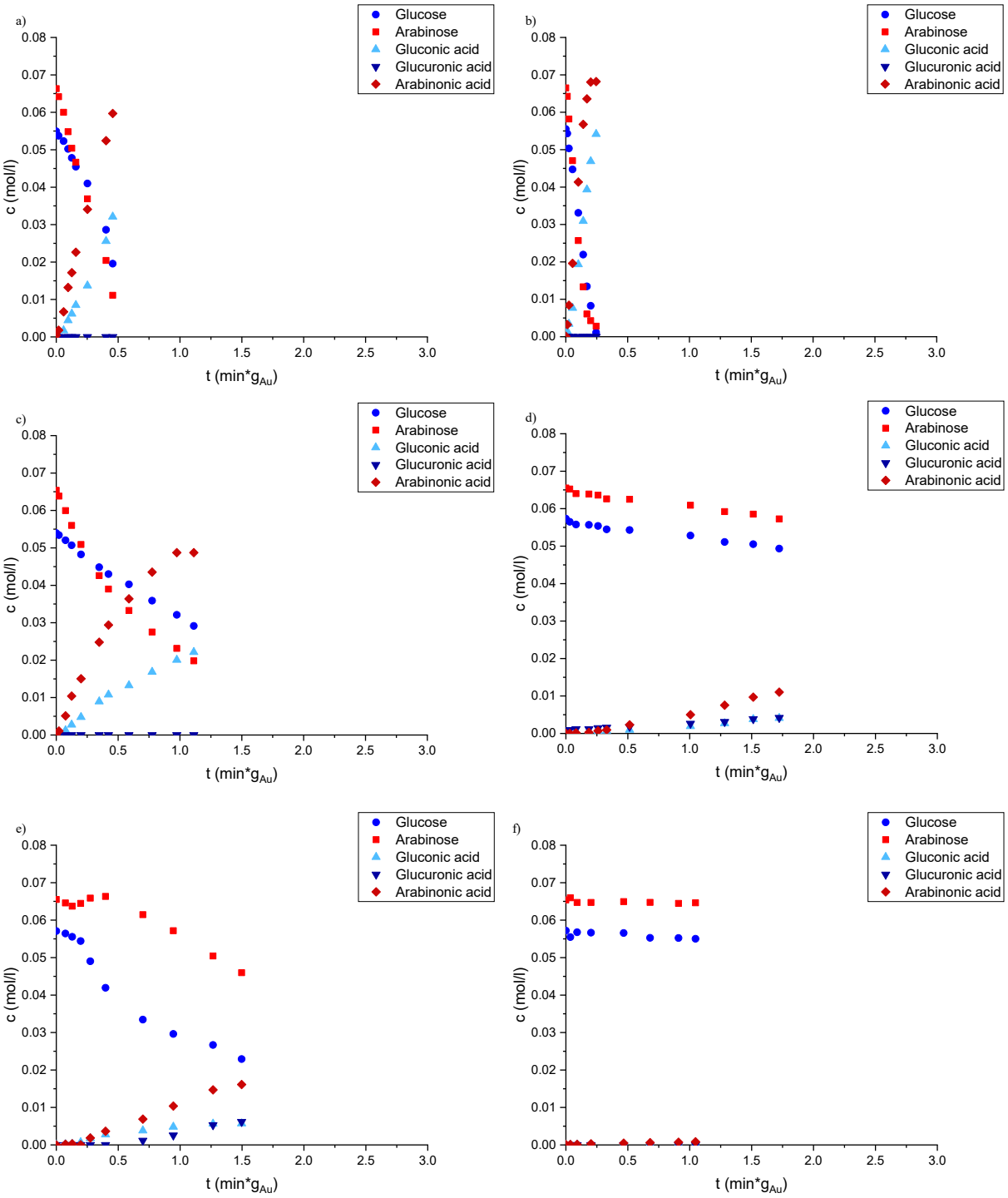

Fig. 3.8. Oxidation of 1:1 arabinose – glucose mixtures at 70 °C, pH 8 and pO_2 = 0.125 atm. Experiments a) to f) are listed in Table 3.2.

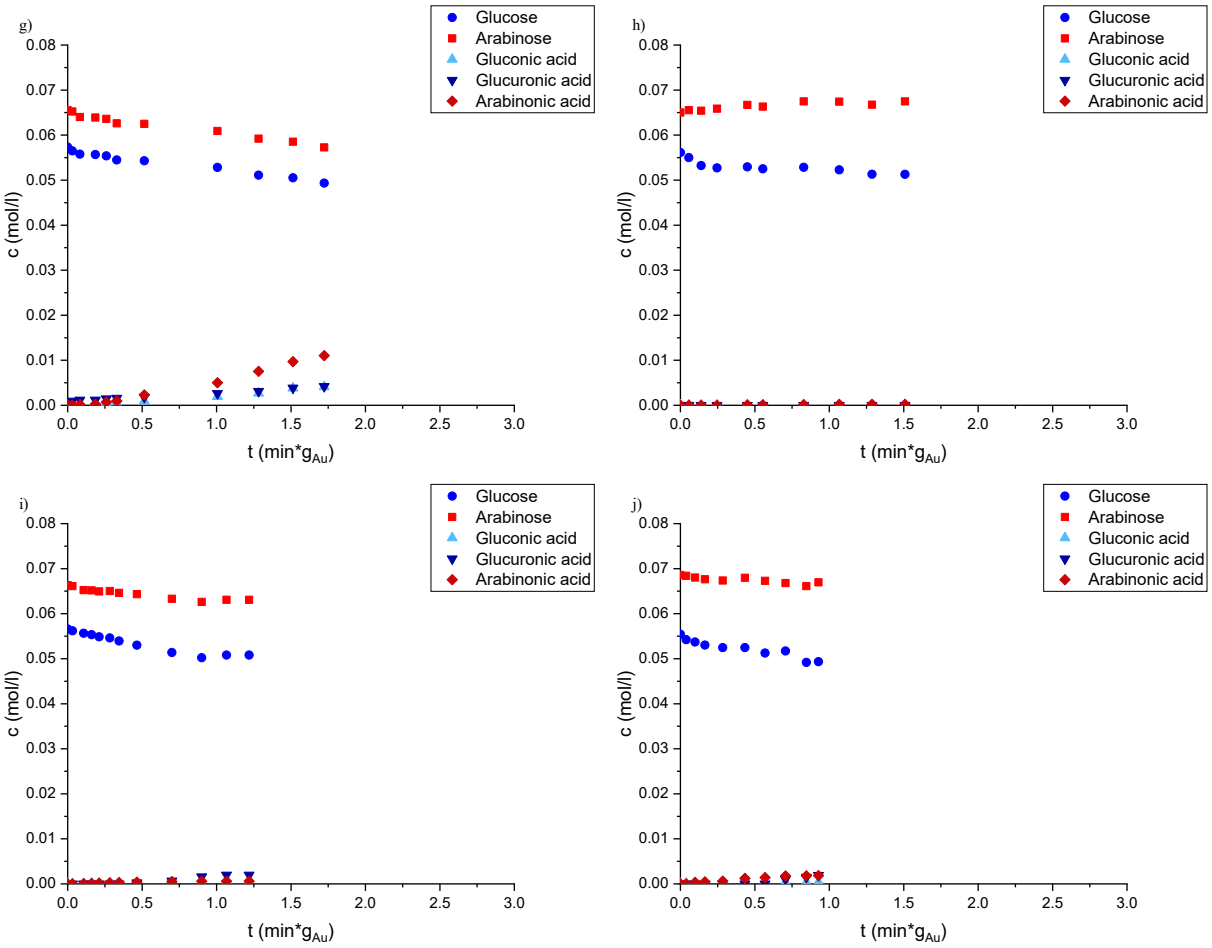

Fig. 3.9. Oxidation of 1:1 arabinose – glucose mixtures at 70 °C, pH 8 and pO_2 = 0.125 atm. Experiments g) to j) are listed in Table 3.2.

3.2.1.1 Comparison of Al_2O_3-supported catalysts

Due to their superior catalytic activity, the three Al_2O_3-supported catalysts were further compared and the rates and selectivity to aldonic acids were determined. Determination of the rate was based on the expression of the nth order rate equation (2).

$$\frac{dc}{dt} = -r = -kc_0^n \tag{2}$$

Parameters k, n and c_0 represent the rate constant, the reaction order and the initial concentration, respectively. The expression for the concentration c as a function of time (3) is obtained by integration of (2).

$$\int_{c_0}^{c} \frac{1}{c^n} dc = \int_0^t -k\, dt \rightarrow c = \sqrt[1-n]{c_0^{1-n} + knt - kt} \tag{3}$$

The Origin software was used for estimation of the parameters k and n to achieve the best fit to the experimental data [43]. The degree of explanation for all evaluations was ≥0.99 and was therefore considered adequate. The rates for catalytic reactions are given in $\frac{\text{mol}}{\text{min g}_{\text{Au}}}$.

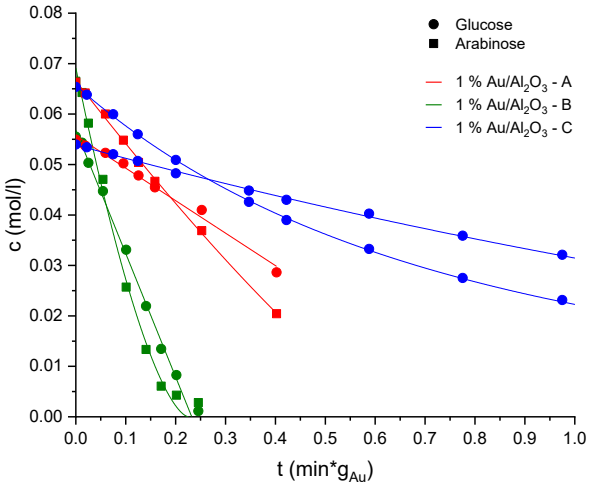

Fig. 3.10. Comparison between results from oxidation of arabinose – glucose mixtures over different Al_2O_3-supported Au catalysts.

Besides the catalytic activity, also selectivity towards the respective aldonic acids is of interest. The selectivity was calculated with equation (4),

$$S_i = \frac{c_{i,X}}{c_{s,0} - c_{s,X}} \cdot 100\% \tag{4}$$

, where $c_{i,X}$ represents the concentration of the aldonic acid at conversion X, and $c_{s,0}$ and $c_{s,X}$ the concentration of the corresponding sugar at the beginning and at conversion X, respectively. Since the peaks of arabinose and fructose overlap during analysis, the selectivity for arabinonic acid is calculated considering $c_{s,X} = c_{Ara,X} + c_{Fruc,X}$. The conversion is determined with (5).

$$X = \left(1 - \frac{c_i}{c_{i,0}}\right) \cdot 100\% \tag{5}$$

The calculated data in Table 3.3 reveals that the rates of 1% Au/Al_2O_3-B for both glucose and arabinose are superior compared to 1% Au/Al_2O_3-A and 1% Au/Al_2O_3-C. The sum of the rates for catalyst B is 0.106 $\frac{\text{mol}}{\text{min g}_{\text{Au}}}$ while the summarized rates are 0.030 $\frac{\text{mol}}{\text{min g}_{\text{Au}}}$ and 0.016 $\frac{\text{mol}}{\text{min g}_{\text{Au}}}$ for catalysts A and C, respectively. A common pattern for all three catalysts is the higher oxidation rate of arabinose compared to glucose. Catalysts A and B displayed a rate

approximately twice as high for arabinose oxidation compared to glucose. Arabinose oxidation proceeds three times more rapidly than oxidation of glucose over catalyst C.

Table 3.3. Calculated and estimated parameters from oxidation of arabinose – glucose mixtures over different Al_2O_3-supported Au catalysts. Rates are calculated for c0 = 0.06 mol/l.

Catalyst	n_{Ara}	k_{Ara} $\left[\frac{mol^{1-n_{Ara}} l^{n_{Ara}}}{min\ g_{Au}}\right]$	n_{Gluc}	k_{Gluc} $\left[\frac{mol^{1-n_{Gluc}} l^{n_{Gluc}}}{min\ g_{au}}\right]$	r_{Ara} $\left[\frac{mol}{min\ g_{Au}}\right]$	r_{Gluc} $\left[\frac{mol}{min\ g_{Au}}\right]$	S_{AraA} (X_{Ara})	S_{GlucA} (X_{Gluc})
A	0.213	0.226	0.000	0.073	0.019	0.011	100% (83%)	91% (64%)
B	0.371	1.312	0.000	0.245	0.069	0.037	100% (96%)	100% (98%)
C	1.380	3.764	0.725	0.224	0.012	0.004	98% (70%)	89% (46%)

Catalyst B showed the highest selectivity to gluconic acid with 100% selectivity at 98% conversion, compared to 91% and 89% for catalysts A and C, respectively. The major by-product in the reactions with catalysts A and C is presumably fructose. However, the influence of fructose decreases at higher conversion and has thus less impact towards full conversion (Section 3.2.2). The selectivity to arabinonic acid was around 100% for all three catalysts.

3.2.2 Influence of catalyst loading

To study the influence of other parameters, it is desired to operate at a catalyst loading where no limitations due to the gas – liquid mass transfer occur. Oxidation reactions of 1:1 arabinose – glucose mass ratio with different catalyst loadings of 1% Au/Al_2O_3-B were performed under the same conditions of 70 °C, pH 8, and pO_2 = 0.125 atm. Plotting the rate against the catalyst loading reveals that the productivity at sugar-to-gold molar ratios above 24000:1 does not significantly change with an increased catalyst loading (Fig. 3.11-left). Consequently, the rate dependent on the mass of catalyst obtains a maximum at 0.1 g catalyst loading. Furthermore, at low catalyst loading the reaction order increases, indicating mass transfer limitations [22]. Accordingly, subsequent experiments were performed at the catalyst loading of 0.1 g.

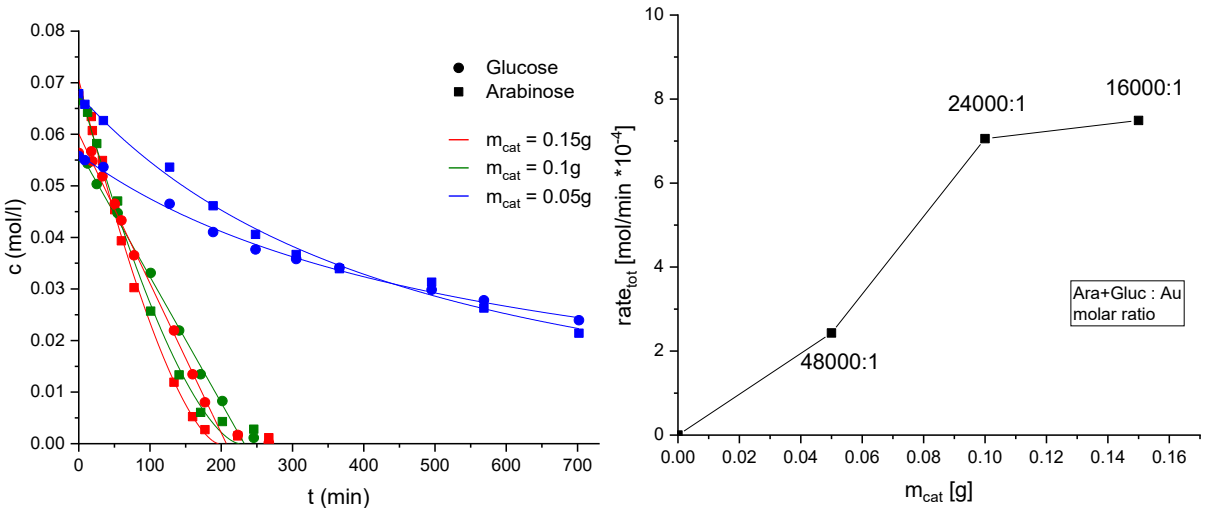

Fig. 3.11. left – Oxidation of arabinose – glucose mixtures over different 1% Au/Al_2O_3-B catalyst loadings at conditions of 1:1 arabinose – glucose mass ratio at 70 °C, pH 8, and pO_2 = 0.125 atm.
right – rates plotted against the catalyst loading. The rates were estimated with to equation (3) and c_0 = 0.06 mol/l for both arabinose and glucose . Labels reflect n_{sugar}:n_{gold} ratios.

3.2.3 Influence of sugar concentrations

In mixtures of arabinose and glucose, the two sugars compete for the adsorption onto the catalyst surface. Thus, different ratios between the sugars may influence adsorption. The concentrations of individual were adjusted by varying the ratios between arabinose and glucose while keeping the total sugar content of 20 g/l. Mixtures with mass fractions of 1, 0.75, 0.5 and 0.25 of both arabinose and glucose, respectively, were investigated (Fig. 3.12). The parameters k and n were evaluated with equation (3) using Origin Software.

As the fraction for glucose decreases, a negative reaction order was observed. For high mass fractions oxidation of arabinose is preferred. With a decreasing amount of arabinose, the rate of glucose oxidation is increasing.

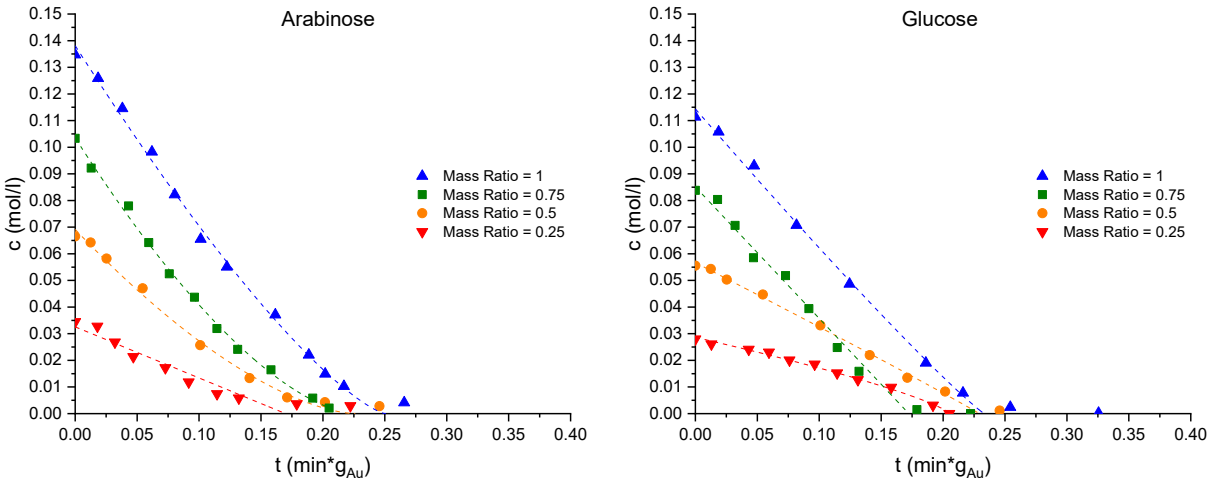

Fig. 3.12. Oxidation of arabinose – glucose mixtures with alternating mass ratios over 1% Au/Al_2O_3-B at 70 °C, pH 8, pO_2 = 0.125 atm and m_{cat} = 0.1 g. The graphs of the individual sugars are kept separate for illustrative purposes.

For mass fractions lower than 1, the rate of arabinose oxidation changes linearly with the mass fraction. However, for solutions with arabinose mass fractions equal to 1, the rate of arabinose is similar to the rate at mass fraction 0.75. Oxidation of glucose reveals the same behavior as for arabinose. For mixtures, the rates for glucose oxidation are approximately half of the rates for arabinose. The highest overall rate was obtained for arabinose – glucose mixture with the mass ratio 3:1, which can be related back to the rates for formations of furanose and open-chain form. For solutions with arabinose mass ratios of 0.75 and higher, the rate for the formation of these components is limiting the oxidation reaction of arabinose. With addition of glucose, the glucofuranose and its acyclic form will also be available on the catalyst surface, increasing the catalytic activity.

Table 3.3. Estimated and calculated parameter values from fitted curves for data from oxidations of arabinose – glucose mixtures. Rates are calculated for c_0 = 0.06 mol/l.

Ara:Gluc		n_{Ara}	k_{Ara} $\left[\frac{mol^{1-n_{Ara}} l^{n_{Ara}}}{min\ g_{Au}}\right]$	n_{Gluc}	k_{Gluc} $\left[\frac{mol^{1-n_{Gluc}} l^{n_{Gluc}}}{min\ g_{au}}\right]$	r_{Ara} $\left[\frac{mol}{min\ g_{Au}}\right]$	r_{Gluc} $\left[\frac{mol}{min\ g_{Au}}\right]$	S_{AraA} (X_{Ara})	S_{GlucA} (X_{Gluc})
Mass ratio	Molar ratio								
1:0	1:0	0.242	1.177	-	-	0.089	-	99% (97%)	-
3:1	0.78:0.22	0.345	1.678	-0.297	0.037	0.095	0.013	98% (98%)	98% (100%)
1:1	0.55:0.45	0.371	1.312	0.000	0.245	0.069	0.037	100% (96%)	100% (98%)
1:3	0.29:0.71	0.000	0.192	0.000	0.494	0.029	0.074	98% (92%)	92.0% (100%)
0:1	0:1	-	-	0.081	0.636	-	0.076	-	96% (100%)

On the contrary, higher glucose fraction decreases the selectivity to gluconic acid, presumably due to an enhanced formation of fructose. Along with the selectivity, the calculated and estimated parameters for the respective reactions are presented in Table 3.3, while the corresponding graphs for each reaction are given in Appendix III.

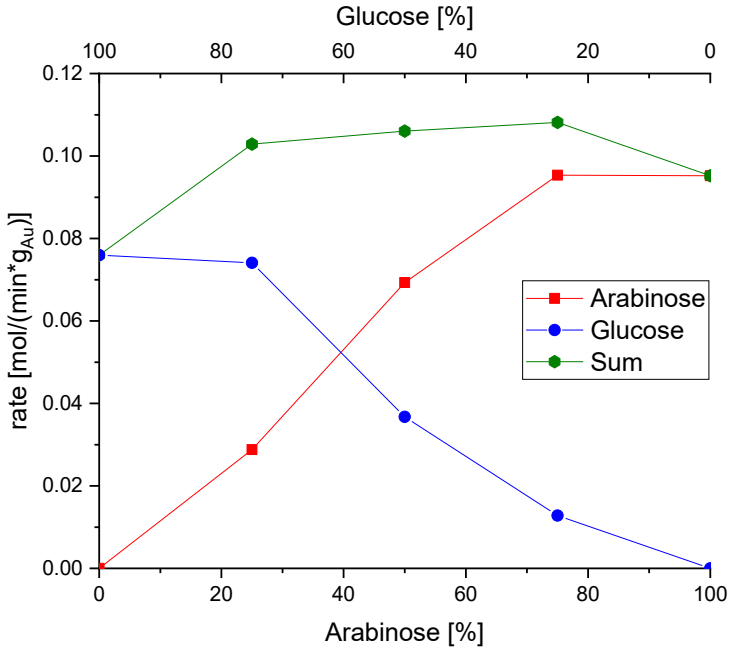

Fig. 3.13. Change in rate of arabinose and glucose oxidation at different mass fractions, respectively, and the summarized overall reaction. The rates are calculated accoding with c_0 = 0.06 mol/l for both arainose and glucose.

For the experiments with only one sugar, no overlapping peaks appear during analysis. Thus, it is possible to observe all products separately and determine a more accurate selectivity towards the aldonic acids. As seen in Fig. 3.14, the selectivity towards the respective aldonic acids is very high. For arabinose, the corresponding lactone appears to some extent, yet rapidly decreasing with time. Furthermore, small quantities of ribulose formation are observed throughout the reaction, decreases, however, towards full conversion of arabinose. For glucose, the most considerable by-product is fructose, which like arabino-δ-lactone only has a greater significance in the beginning, decreasing with conversion.

An unidentified product was observed for both arabinose and glucose oxidation. It is hypothesized that this product reflects a formation of oligomers, as it during analysis appears at similar retention times as confirmed oligomers (6.2 min). Graphs from HPLC analysis for both reactions are presented Appendix IV.

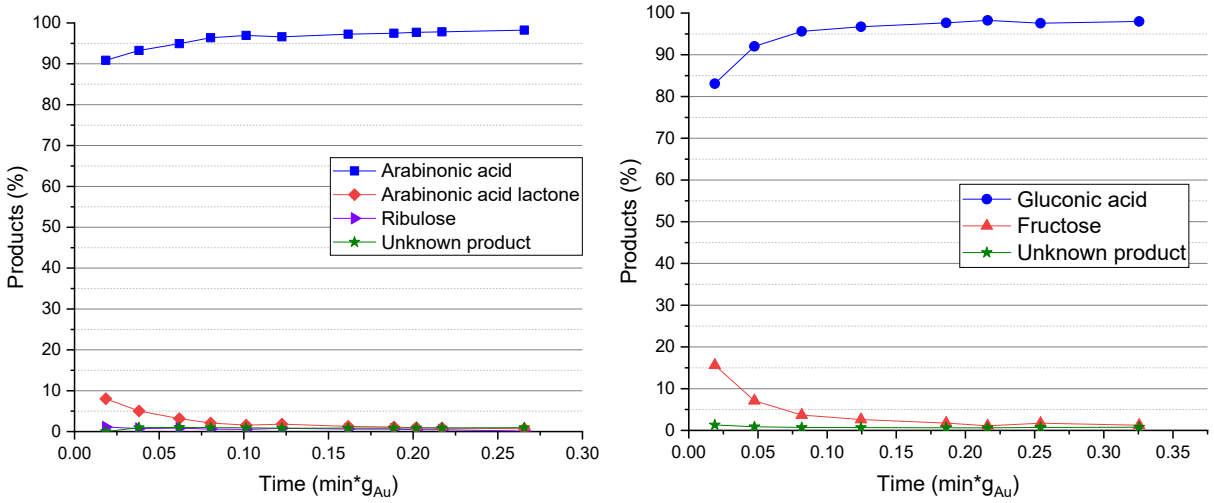

Fig. 3.14. Percentage of individual products over reaction timeline for oxidation of 1:0 (left) and 0:1 (right) arabinose – glucose mass ratios over 1% Au/Al_2O_3-B.

3.2.4 Influence of temperature

Oxidation of arabinose over gold nanoparticles had earlier been conducted at 60 °C [13]. In this work, for comparison, the reaction temperature interval from 50-80 °C was studied. Besides the increase in catalytic activity with temperature according to Arrhenius' equation, as discussed in Section 1.3, the mutarotation equilibrium is slightly shifted with temperature towards a higher furanose fraction, hence giving a higher amount of reactive compounds. On the contrary, the gas – liquid solubility follows the equation for temperature and pressure dependent gas solubility in water (6) [44], thus suffering with increased temperature. The temperature T is in Kelvin (K).

$$c_{O_2} = p_{O_2}\, e^{\frac{0.046T^2+203.35T\ln\left(\frac{T}{298}\right)-(299.378+0.092T)(T-298)-20.591\cdot10^3}{8.3144T}} \qquad (6)$$

Reactions with varying temperature were performed at pH 8, pO_2 = 0.125 atm and the catalyst loading of 0.1 g of 1% Au/Al_2O_3-B. The arabinose to glucose mass ratio was 1:1, yet for illustrative purposes, the reactions for arabinose and glucose are split into separate graphs (Fig. 3.15). Another representation is shown in Appendix V.

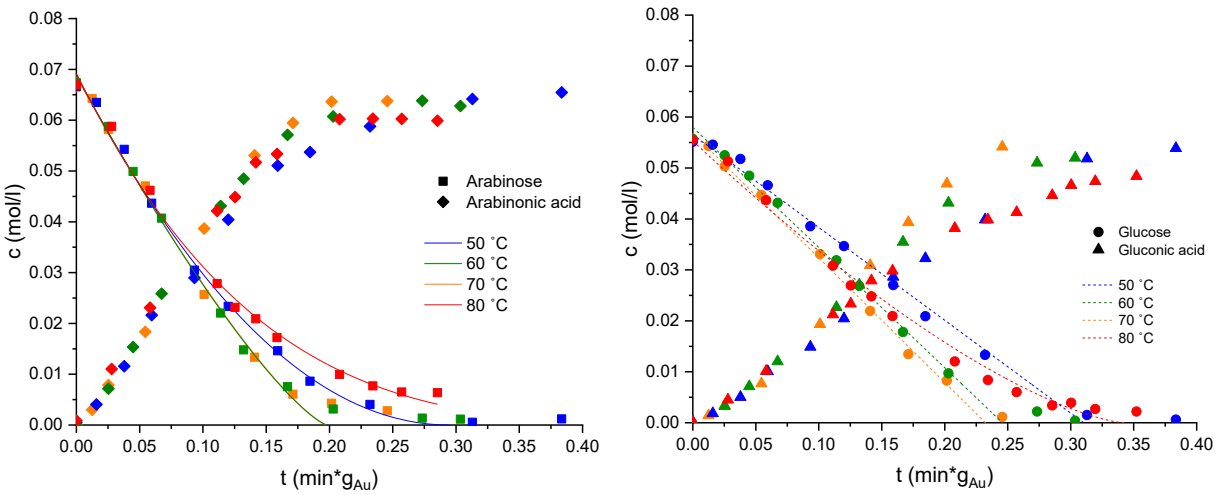

Fig. 3.15. Influence of temperature on oxidation of 1:1 arabinose – glucose mixtures over 1% Au/Al_2O_3-B at pH 8, 0.125 atm pO_2 and a catalyst loading of 0.1 g. Dotted lines represent calculations.

As expected, the trend shows an increasing rate with temperature, although identical results at 60 and 70 °C for arabinose oxidation were observed (Table 3.4). However, at 80 °C a decrease in the overall rate was observed, thus giving the maximum rate at 70 °C for glucose and at 60-70 °C for arabinose. The same behavior and maximum were observed for catalyst 1% Au/Al_2O_3-A. Overall, temperature had a larger impact on glucose than on arabinose oxidation. Furthermore, lower selectivity towards gluconic acid was obtained especially at temperatures above 70 °C. The selectivity to gluconic acid was noticeably lower at 80 °C than at temperatures below 70 °C. Thus, the apparent activation energy (E_a) is calculated from the linearized form of the Arrhenius equation (7) without considering the data at 80 °C.

$$\ln k = \ln A - \frac{E_a}{R}\frac{1}{T} \tag{7}$$

During parameter estimation with equation (3), since only the rate constant is dependent on the temperature, the reaction order was kept constant according to the value estimated at 70 °C, i.e. n_{Ara}=0.371 and n_{Gluc}=0.000 (Section 3.2.3).

Table 3.4. Estimated and calculated parameters for oxidation reactions of arabinose – glucose mixtures at temperatures ranging from 50-80 °C over 1% Au/Al_2O_3-B. k_i – rate constant, r – rate, S_i – selectivity, X_i – conversion. Rates are calculated for c_0 = 0.06 mol/l, n_{Ara} = 0.371 and n_{Gluc} = 0.000.

T [°C]	k_{Ara} $\left[\frac{mol^{0.629}l^{0,371}}{min\ g_{Au}}\right]$	k_{Gluc} $\left[\frac{mol}{min\ g_{Au}}\right]$	r_{Ara} $\left[\frac{mol}{min\ g_{Au}}\right]$	r_{Gluc} $\left[\frac{mol}{min\ g_{Au}}\right]$	S_{AraA} (X_{Ara})	S_{GlucA} (X_{Gluc})
50	1.159	0.191	0.061	0.029	99% (99%)	99% (99%)
60	1.325	0.236	0.070	0.035	96% (98%)	94% (99%)
70	1.312	0.245	0.069	0.037	100% (96%)	100% (98%)
80	1.050	0.201	0.055	0.030	100% (91%)	91% (96%)

The plot in Fig. 3.16 shows that oxidation of glucose is more influenced by temperature than of arabinose. E_a for glucose oxidation was around 11.7 $\frac{kJ}{mol}$, while being closer to 6.8 $\frac{kJ}{mol}$ for arabinose oxidation. Common for both, however, is that these values differ remarkably from values reported in literature. Kusema et al. reported an E_a for arabinose at around 24 $\frac{kJ}{mol}$, while an E_a of 27 $\frac{kJ}{mol}$ was reported by Ishida et al. for oxidation of glucose [21, 45]. The results allow to consider that at the given conditions, temperature differences from 50-70 °C have low effect on oxidation reactions of the mixture. Above 70 °C, changes in the rate and reaction order occur. The decreased rate at temperatures from 80 °C could be explained by the decreased solubility of oxygen or sugar disproportionation, leading to catalyst coking [46].

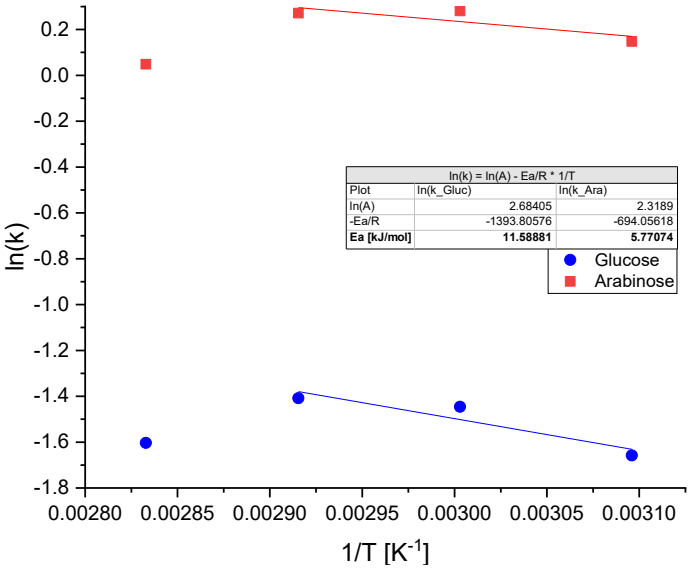

Fig. 3.16. Arrhenius plot for oxidation of 1:1 arabinose – glucose mixtures over 1% Au/Al2O3-B.

3.2.5 Influence of pH

Oxidation of aldoses gives aldonic and uronic acids and thus a decrease in pH, causing not only a decreased rate, but also potentially catalyst deactivation. Low pH enhances adsorption of the acids on the catalyst, hindering adsorption of reactants and suppressing the reaction [21]. With increased pH, the ring-opening process of the lactones is favored and thus a higher yield of aldonic acids is obtained. For glucose, it has been reported that from neutral pH values, conversion of lactone into glucuronic acid increases rapidly [47]. However, high pH values promote the formation of by-products. For example, an increase in pH enhances the isomerization of glucose to fructose.

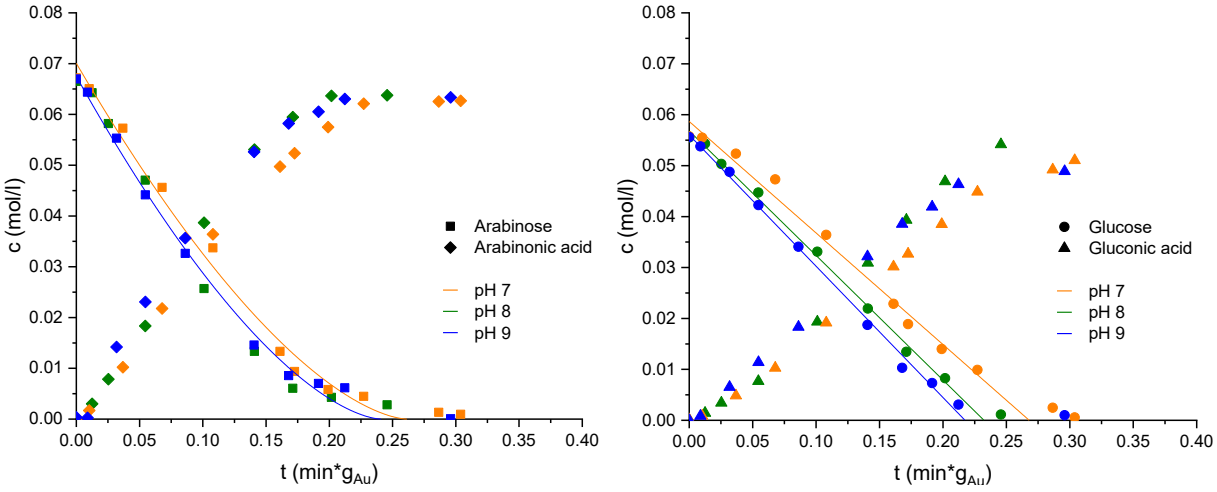

Fig. 3.17. Oxidation of 1:1 arabinose – glucose mixtures over 1% Au/Al_2O_3-B at different pH values and conditions of 70 °C, pO_2 = 0.125 atm and m_{cat} = 0.1 g. For illustrative purposes, the two sugars are shown in separate graphs (left – arabinose, right – glucose).

Three experiments at pH values 7, 8 and 9 were conducted under the same conditions of 1:1 arabinose – glucose mass ratio, 70 °C, pO_2 = 0.125 atm and m_{cat} = 0.1 g (Fig. 3.17). It was considered that the isomerization to fructose would play a significant role at pH values from 10 and above, hence no experiments at higher pH were performed. In other studies, reporting arabinose oxidation under similar conditions, pH in this range had a significant impact on the reaction [21]. However, in the current work no major influence of pH on the reaction was noticed. For arabinose, pH 8 and 9 displayed close to identical results, while the reaction proceeded slightly less slowly at pH 7 (Fig. 3.18). Glucose showed equivalent results, where the rates at pH 8 and 9 were akin and slightly lower at pH 7. The highest selectivity towards gluconic acid was obtained at pH 8. At 9 the selectivity to gluconic acid suffered presumably

due to a higher isomerization rate to fructose. Specific values are given in Table 3.5. At pH 7, the lower selectivity to aldonic acids could be explained by a decreased rate of the lactone ring-opening.

Table 3.5. Estimated and calculated parameters for oxidation of arabinose – glucose mixtures at different pH values. k_i – rate constant, r – rate, S_i – selectivity, X_i – conversion. Rates are calculated for c_0 = 0.06 mol/l, n_{Ara} = 0.371 and n_{Gluc} = 0.000.

pH	k_{Ara} $\left[\frac{mol^{0.629}l^{0,371}}{min\ g_{Au}}\right]$	k_{Gluc} $\left[\frac{mol}{min\ g_{Au}}\right]$	r_{Ara} $\left[\frac{mol}{min\ g_{Au}}\right]$	r_{Gluc} $\left[\frac{mol}{min\ g_{Au}}\right]$	S_{AraA} (X_{Ara})	S_{GlucA} (X_{Gluc})
7	1.142	0.219	0.060	0.033	95% (99%)	92% (99%)
8	1.312	0.245	0.069	0.037	100% (96%)	100% (98%)
9	1.210	0.258	0.064	0.039	95% (100%)	90% (98%)

Fig. 3.18. Projection of rates vs pH and selectivity vs pH. Rates are calculated with c_0 = 0.06 mol/l.

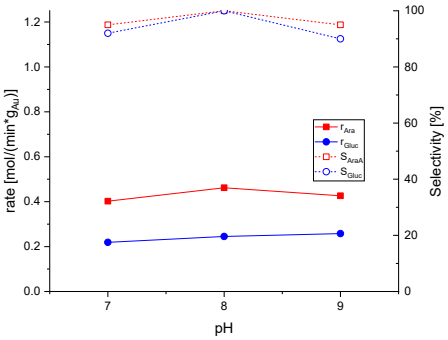

3.2.6 Influence of oxygen pressure

It has earlier been mentioned that gold does not undergo over-oxidation and thus, an excess in oxygen will not induce catalyst deactivation. However, due to the adsorption of oxygen onto the active sites, an excessive concentration of oxygen may lead to lower availability of active sites to sugar molecules, diminishing the oxidation rate.

Since oxygen also is a reactive component, the rate equation for the nth order is modified to also include the oxygen concentration as a parameter. Earlier, as the oxygen concentration was constant it was included into the rate constant k in equation (3). Now, k is further fractionated according to equation (8), where k' reflects the rate constant independent on the oxygen concentration, c_{O_2} the oxygen concentration and n_{O_2} the reaction order for oxygen.

$$k = k' * c_{O_2}^{n_{O_2}} \tag{8}$$

By logarithmic linearization of (8), n_{O_2} and k' can be determined (9).

$$\ln k = \ln k' + n_{O_2} c_{O_2} \tag{9}$$

To investigate the actual influence of oxygen pressure on the reaction, three experiments with varying pressures (pO_2 = [0.0625; 0.125; 0.250] atm) were carried out at 70 °C, pH 8 and m_{cat} = 0.1 g (Fig. 3.19).

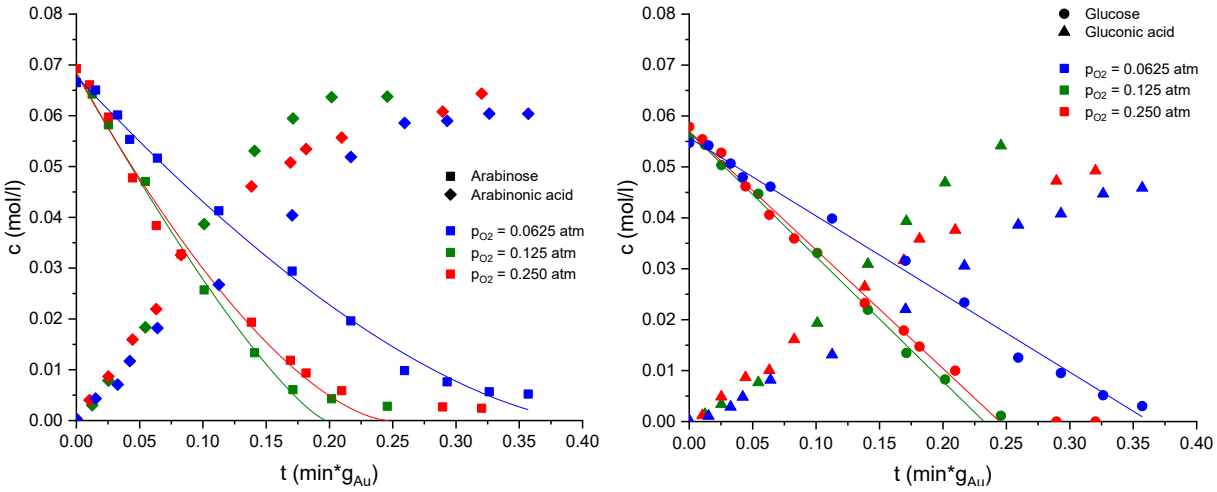

Fig. 3.19. Oxidation of 1:1 arabinose – glucose mixtures over 1% Au/Al_2O_3-B at different oxygen pressures and conditions of 70 °C, pH 8 and m_{cat} = 0.1 g. For illustrative purposes, the sugars are displayed in separate graphs. The lines represent the rate calculated with equation (3).

While oxygen concentration increases linearly, the oxidation rates of arabinose and glucose does not follow the same trend (Table 3.6). At oxygen pressures below 0.125 atm, a clear insufficiency of oxygen is observed, indicating the presence of gas – liquid mass transfer limitations and thus decelerating the reaction. On the contrary, at oxygen pressures over 0.125 atm the rate slightly started decreasing, resulting in a rate maximum at 0.125 atm. At oxygen pressures above 0.125 atm, the high concentration of oxygen results in a large amount of adsorbed oxygen, thus hindering the adsorption of the monosaccharides and limiting the reaction.

Consequently, for both arabinose and glucose, the application of equation (8) results in n_{O_2} values of approximately 1.2±1 (Fig. 3.20). When investigating the rates in Table 3.6, it also becomes apparent that oxidation of arabinose is slightly more sensitive to the concentration of oxygen compared to oxidation of glucose.

Table 3.6. Data obtained from oxidation of arabinose - glucose mixture under different oxygen pressures. p_{O_2} – oxygen pressure, c_{O_2} – concentration of oxygen in the liquid phase calculated with equation (6), S_i – selectivity, X – conversion, r_i – rate for c_0 = 0.06 mol/l, n_{Ara} = 0.371 and n_{Gluc} = 0.000.

p_{O_2} [atm]	c_{O_2} $\left[\frac{mmol}{l}\right]$	k_{Ara} $\left[\frac{mol^{0,629}l^{0,371}}{min\ g_{Au}}\right]$	k_{Gluc} $\left[\frac{mol}{min\ g_{au}}\right]$	r_{Ara} $\left[\frac{mol}{\text{min}\ g_{Au}}\right]$	r_{Gluc} $\left[\frac{mol}{\text{min}\ g_{Au}}\right]$	S_{AraA} (X_{Ara})	S_{GlucA} (X_{Gluc})
0.0625	0.0512	0.726	0.153	0.038	0.023	98% (92%)	89% (94%)
0.125	0.1024	1.312	0.245	0.069	0.037	100% (96%)	100% (98%)
0.250	0.2048	1.190	0.233	0.063	0.035	96% (97%)	85% (100%)

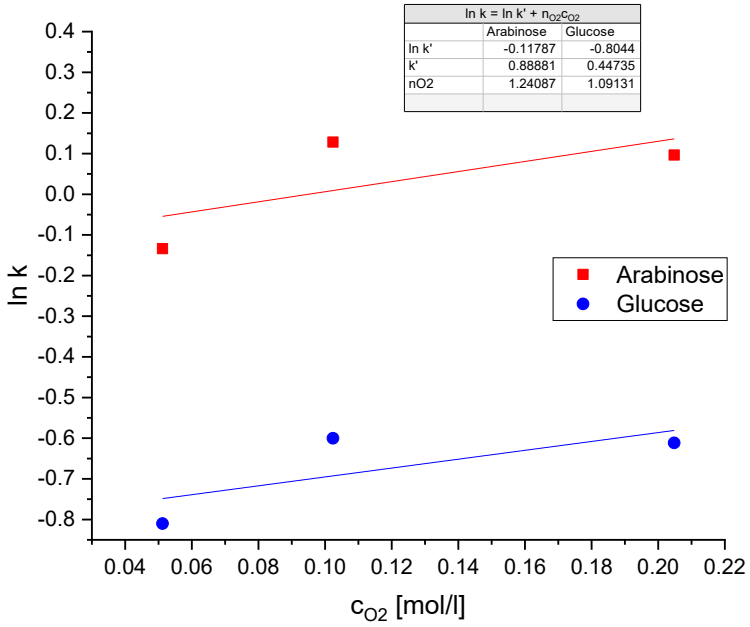

Fig. 3.20. Linearization of equation (8) for determination of n_{O_2} and k'.

In terms of selectivity, compared to the high selectivity at 0.125 atm, significantly lower selectivity to gluconic acid was achieved at 0.250 atm, followed by 0.0625 atm. Because arabinose is the favored adsorbed molecule, the high oxygen content at 0.250 atm may induce less available sites, which further hinders glucose adsorption and oxidation and instead enhances fructose formation. Additionally, this hypothesis would be supported by the high selectivity to arabinonic acid observed at all oxygen pressures.

3.2.7 Catalyst stability

Catalyst deactivation implies a loss of catalytic activity and/or selectivity over time. A stable catalyst shows no or very minimal catalyst deactivation. Catalyst stability is important from both an economic point of view and practical viewpoints.

Reasons for catalyst deactivation in heterogeneous solid – liquid reactions can be coking, meaning the formation of carbon on the catalyst surface, sintering of the metal particles to larger clusters due to high temperatures, leaching of the active metal into the liquid phase, poisoning and transformations of the active phase, e.g. oxidation of the metal. As mentioned in Section 1.2, gold has the advantage of not over-oxidizing by oxygen. pH affects not only the rate, but also the stability of Au catalysts, i.e. lower pH shortens the catalyst lifetime, reportedly [48]. Occasionally, deactivated catalysts can be regenerated to improve activity, for example, coke can be burnt off. The initial catalytic activity is, however, usually never retained. On the contrary, leaching and sintering are generally irreversible.

In continuous systems, catalyst deactivation can easily be detected by decreased conversion or change in selectivity. For batch reactions, the catalyst is recycled and used again in a reaction with the same conditions. In the current work, 0.1 g 1% Au/Al_2O_3-B catalyst was used in the oxidation reaction with the mass ratio of 1:1 for the arabinose – glucose mixture at 70 °C, pH 8 and pO_2 = 0.125 atm. After the reaction, the catalyst was washed and recycled. The recycled dry catalyst weighted 0.086 g and the loss in catalyst mass was considered by multiplying time with the mass of gold. For graphical comparison, the results are displayed in Fig. 3.21.

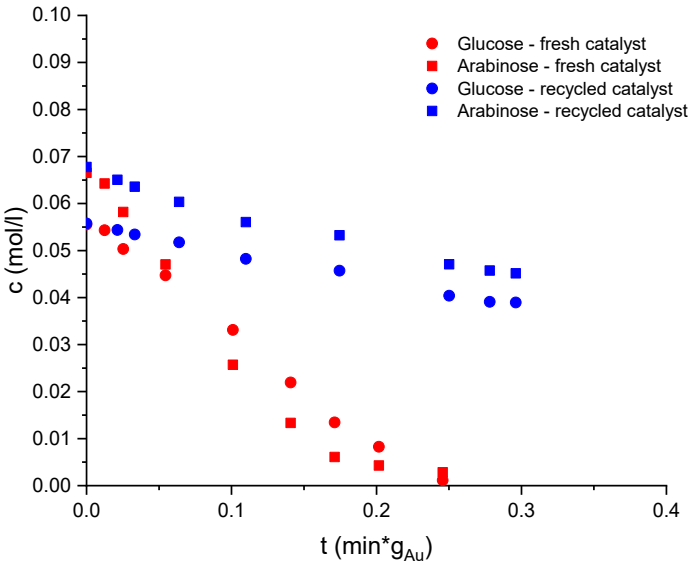

Fig. 3.21. Comparison between oxidation of the arabinose – glucose mixture over fresh vs. recycled 1% Au/Al_2O_3-B catalyst under conditions of 70 °C, pH 8, pO_2 = 0.125 atm and mass ratio 1:1 arabinose – glucose.

The results clearly display presence of deactivation for the recycled catalyst. Due to the low temperatures, a possibility of sintering is fairly low. Relating back

to Section 3.1, where it was observed that the spent catalyst did not contain as many large particles as the fresh catalyst, a strong hypothesis was leaching of Au into the liquid. ICP-MS analysis, however, showed only very minor content of gold in the liquid close to the lower limit of detection (Appendix VI). Therefore, catalyst coking is suspected, which should be further investigated.

3.3 Kinetic modelling

A well-structured model for catalytic arabinose oxidation has earlier been demonstrated by Correia et al. [13], which is partially based on the model presented by Kusema et al. [49]. In this work, the presented model was used as a basis and extended for the simultaneous oxidation of arabinose and glucose. The routes in the model presented in [13] are inspired by the oxidation routes of glucose. Hence, no interferences regarding the use of this model as a basis for the modelling of the simultaneous oxidation of arabinose and glucose were concluded. The reaction routes and steps are listed in Table 3.8 for which the nomenclature is found in Table 3.7.

Table 3.7. Nomenclature for reaction steps and routes in Table 3.8.

Reaction step designation	Component	Abbreviation
*	Active site	-
RCHO	Glucose	Gluc
RCO	Glucono-γ-lactone	-
GlucL	Glucono-δ-lactone	GlucL
RCOOH	Gluconic acid	GlucA
$RCOO^-$	Gluconate	GlucO
$RCOHOH^-$	Dehydrated glucose aldehydrol	-
RCHOHOH	Glucose aldehydrol	GlucOH
R'CHO	Arabinose	Ara
R'CO	Arabino-γ-lactone	-
AraL	Arabino-δ-lactone	AraL
R'COOH	Arabinonic acid	AraA
$R'COO^-$	Arabinonate	AraO
$R'COHOH^-$	Dehydrated arabinose aldehydrol	-
R'CHOHOH	Arabinose aldehydrol	AraOH
Fruc	Fructose	Fruc
Rib	Ribulose	Rib

For both arabinose and glucose, two mechanisms have been developed for the oxidation to their corresponding aldonic acids and subsequently to their anionic form. For glucose, the mechanism contains three routes N^i and four routes for arabinose. Additionally, the

isomerization process of glucose to fructose and the potential isomerization of arabinose to ribulose are also considered as routes.

All adsorption – desorption reaction steps (1, 2, 5, 10, 13, 15, 18, 23, 26, 28) are considered to rapidly be at quasi-equilibrium, not significantly influencing the overall reaction rates [13]. Reaction steps 4, 6, 7, 9, 12, 17, 20, 22 and 25 are expected to be fast, not affecting the rates. Hence, in route N^{I}, reflecting the oxidation of glucose to gluconic acid proceeding via the lactone form, the critical step is the reaction between adsorbed glucose and adsorbed molecular oxygen (step 3). Under the reaction conditions used in this work, oxygen is considered to be molecular adsorbed, as stated in [50]. Routes N^{II} and N^{III} describe the mechanism starting from acyclic glucose. In N^{II}, glucose is via a nucleophilic attack in alkaline environment rapidly converted to its aldehydrol form. The step determining the rate of the route is the nucleophilic attack (step 8). Route N^{III} reflects the subsequent oxidation of the adsorbed aldehydrol (step 11). Route N^{IV} reflects the homogeneous catalyzed isomerization of glucose to fructose.

The fifth route, N^{V}, describes the oxidation of arabinose to arabino-δ-lactone. After the reaction between arabinofuranose and oxygen (step 16), both in adsorbed state, the ring of the resulting arabino-γ-lactone is rapidly conformed to arabino-δ–lactone as an intermediate. Route N^{VI} reflects the subsequent ring-opening of the lactone in alkaline environment (step 19) and is a reaction with H_2O. However, as water is in excess, the reaction is dependent on the availability of hydroxide [13].

Routes N^{VII} and N^{VIII} represent the oxidation of arabinose proceeding via the aldehydrol of arabinose. First, arabinose is attacked by a nucleophile, hydroxide, and converted to its aldehydrol (step 21). Subsequently, the adsorbed aldehydrol reacts with oxygen to arabinonic acid (step 24) and later to arabinonate in route N^{VII}. Finally, N^{IX} reflects the heterogeneously catalyzed isomerization of arabinose to ribulose.

Reaction steps 4, 12, 16 and 24 give hydrogen peroxide as a by-product. It is, however, noteworthy that during analysis no H_2O_2 was detected, presumably due to its unstable nature in aqueous and alkaline environment.

Table 3.8. Reaction steps (1 – 28) and routes (N^i) for simultaneous oxidation of arabinose – glucose mixture over Au/Al_2O_3-B. The nomenclature is given in Table 3.7.

		N^{I}	N^{II}	N^{III}	N^{IV}	N^{V}	N^{VI}	N^{VII}	N^{VIII}	N^{IX}
1	RCHO + * ↔ RCHO*	1	0	0	0	0	0	0	0	0
2	O_2 + * ↔ O_2*	1	0	1	1	0	0	1	0	0
3	RCHO* + O_2* → RCO* + OOH*	1	0	0	0	0	0	0	0	0
4	RCO* + HOO* $\xrightarrow{fast}$ GlucL + H_2O_2 + *	1	0	0	0	0	0	0	0	0
5	GlucL* ↔ GlucL + *	1	0	0	0	0	0	0	0	0
6	GlucL + H_2O $\xrightarrow{fast,\ OH^-}$ RCOOH	1	0	0	0	0	0	0	0	0
7	RCOOH + OH^- $\xrightarrow{fast}$ $RCOO^-$ + H_2O	1	0	1	0	0	0	0	0	0
8	RCHO + OH^- ↔ $RCOHOH^-$	0	1	0	0	0	0	0	0	0
9	$RCOHOH^-$ + H^+ $\xrightarrow{fast}$ RCHOHOH	0	1	0	0	0	0	0	0	0
10	RCHOHOH + * ↔ RCHOHOH*	0	0	1	0	0	0	0	0	0
11	RCHOHOH* + O_2* → RCOHOH* + OOH*	0	0	1	0	0	0	0	0	0
12	RCOHOH* + OOH* $\xrightarrow{fast}$ RCOOH* + H_2O_2 + *	0	0	1	0	0	0	0	0	0
13	RCOOH* ↔ RCOOH + *	0	0	1	0	0	0	0	0	0
14	RCHO ↔ Fruc	0	0	0	1	0	0	0	0	0
15	R'CHO + * ↔ R'CHO*	0	0	0	0	1	0	0	0	1
16	R'CHO* + O_2* → R'CO* + OOH*	0	0	0	0	1	0	0	0	0
17	R'CO* + OOH* $\xrightarrow{fast}$ AraL + H_2O_2 + *	0	0	0	0	1	0	0	0	0
18	AraL* ↔ AraL + *	0	0	0	0	1	0	0	0	0
19	AraL + H_2O $\xrightarrow{OH^-}$ R'COOH	0	0	0	0	0	1	0	0	0
20	R'COOH + OH^- $\xrightarrow{fast}$ $R'COO^-$ + H_2O	0	0	0	0	0	1	0	1	0
21	R'CHO + OH^- ↔ $R'COHOH^-$	0	0	0	0	0	0	1	0	0
22	$R'COHOH^-$ + H^+ $\xrightarrow{fast}$ R'CHOHOH	0	0	0	0	0	0	1	0	0
23	R'CHOHOH + * ↔ R'CHOHOH*	0	0	0	0	0	0	0	1	0
24	R'CHOHOH* + O_2* → R'COHOH* + OOH*	0	0	0	0	0	0	0	1	0
25	R'COHOH* + OOH* $\xrightarrow{fast}$ R'COOH* + H_2O_2 + *	0	0	0	0	0	0	0	1	0
26	R'COOH* ↔ R'COOH + *	0	0	0	0	0	0	0	1	0
27	R'CHO* ⟶ Rib*	0	0	0	0	0	0	0	0	1
28	Rib*↔ Rib + *	0	0	0	0	0	0	0	0	1

N^{I}	Gluc + O_2 $\xrightarrow{OH^-}$ GlucO + H_2O_2	N^{V}	Ara + O_2 ⟶ AraL + H_2O_2
N^{II}	Gluc + H_2O ⟶ GlucOH	N^{VI}	AraL + OH^- ⟶ AraO
N^{III}	GlucOH + O_2 ⟶ GlucO + H_2O_2	N^{VII}	Ara + H_2O ⟶ AraOH
N^{IV}	Gluc ↔ Fruc	N^{VIII}	AraOH + O_2 ⟶ AraO + H_2O_2
		N^{IX}	Ara ⟶ Rib

Accordingly, the kinetic model comprises of the critical steps: furanose oxidations (steps 3 and 15), aldehydrol formations (steps 8 and 21) aldehydrol oxidations (steps 11 and 24) as well as the ring-opening of arabino-δ-lactone (step 19) and the isomerization to fructose (step 14) and ribulose (step 27). On this basis, the rate equations are derived (10)-(18).

$$r_I = r_3 = k_3 \theta_{Gluc} \theta_{O_2} \tag{10}$$

$$r_{II} = r_8 = k_8 c_{Gluc} c_{OH^-} - k_{-8} c_{GlucOH} \tag{11}$$

$$r_{III} = r_{11} = k_{11} \theta_{GlucOH} \theta_{O_2} \tag{12}$$

$$r_{IV} = r_{14} = k_{14} c_{Gluc} - k_{-14} c_{Fruc} \tag{13}$$

$$r_V = r_{16} = k_{16} \theta_{Ara} \theta_{O_2} \tag{14}$$

$$r_{VI} = r_{19} = k_{19} c_{AraL} c_{OH^-} \tag{15}$$

$$r_{VII} = r_{21} = k_{21} c_{Ara} c_{OH^-} - k_{-21} c_{AraOH} \tag{16}$$

$$r_{VIII} = r_{24} = k_{24} \theta_{AraOH} \theta_{O_2} \tag{17}$$

$$r_{IX} = r_{27} = k_{27} \theta_{Ara} \tag{18}$$

$r_I - r_{XI}$ reflect rates along the corresponding routes, comprised of the rates of the critical steps in the routes; r_3, r_8, r_{11}, r_{14}, r_{16}, r_{19}, r_{21}, r_{24} and r_{27}, respectively. Parameter θ_i describes the fraction of sites occupied by component i. It is important to note that these reactions are based on batch reactions with fresh catalyst. Thus, any influence of deactivation was disregarded. Equations r_3, r_{11}, r_{16} and r_{24} can be rewritten incorporating the Langmuir adsorption isotherm (19),

$$\theta_i = \frac{K_i c_i}{1 + \sum Kc} = K_i c_i \theta_0 \tag{19}$$

, where the term θ_0 describes the fraction of vacant sites (20), K_i the adsorption equilibrium constant, and c_i the concentration of component i. $\sum Kc$ defines the sum of the products of the equilibrium constants (21) and concentrations for each component.

$$\theta_0 = \frac{1}{1 + \sum Kc} \tag{20}$$

$$\begin{aligned} \sum Kc = {} & K_{O_2} c_{O_2} + K_{Gluc} c_{Gluc} + K_{GlucOH} c_{GlucOH} + K_{GlucA} c_{GlucA} + K_{Fruc} c_{Fruc} \\ & + K_{GlucL} c_{GlucL} + K_{Ara} c_{Ara} + K_{AraOH} c_{AraOH} + K_{AraA} c_{AraA} + K_{AraL} c_{AraL} \\ & + K_{Rib} c_{Rib} \end{aligned} \tag{21}$$

The rewritten rates are now dependent on the concentration profiles and the fraction of vacant sites (22)-(26). The adsorption equilibrium constants are embedded into the modified rate constants k'_i. This is done to achieve a better parameter estimation [13].

$$r_I = k'_3 c_{Gluc} c_{O_2} \theta_0 \tag{22}$$

$$r_{III} = k'_{11} c_{GlucOH} c_{O_2} \theta_0 \tag{23}$$

$$r_V = k'_{16} c_{Ara} c_{O_2} \theta_0 \tag{24}$$

$$r_{VIII} = k'_{24} c_{AraOH} c_{O_2} \theta_0 \tag{25}$$

$$r_{XI} = k'_{27} c_{Ara} \theta_0 \tag{26}$$

The concentration of hydroxide is obtained from equation (27) and is constant with the set pH. The concentration of oxygen is calculated from equation (6).

$$c_{OH^-} = 10^{-(14-pH)} \tag{27}$$

To account for the catalyst mass dependence of the rates r_I, r_{III}, r_V and r_{VIII}, the reference catalyst bulk density ρ_{ref} was introduced (28)-(32) . ρ_{ref} is defined as the ratio between the mass of active metal in the catalyst, i.e. mass of gold, and the reaction volume. In this case, 0.1 g catalyst mass was used as a reference, thus giving $\rho_{ref} = 0.0067$ g/l.

$$r_{I,ref} = \frac{r_I}{\rho_{ref}} = \frac{k_3 c_{Gluc} c_{O_2} \theta_0}{\rho_{ref}} \tag{28}$$

$$r_{III,ref} = \frac{r_{III}}{\rho_{ref}} = \frac{k_{11} c_{GlucOH} c_{O_2} \theta_0}{\rho_{ref}} \tag{29}$$

$$r_{V,ref} = \frac{r_V}{\rho_{ref}} = \frac{k_{16} c_{Ara} c_{O_2} \theta_0}{\rho_{ref}} \tag{30}$$

$$r_{VIII,ref} = \frac{r_{VIII}}{\rho_{ref}} = \frac{k_{24} c_{AraOH} c_{O_2} \theta_0}{\rho_{ref}} \tag{31}$$

$$r_{XI,ref} = \frac{r_I}{\rho_{ref}} = \frac{k_{27} c_{Ara} c_{O_2} \theta_0}{\rho_{ref}} \tag{32}$$

All kinetic constants k_i are dependent on temperature and the activation energy ($E_{a,i}$). Applying Arrhenius law, the activation energy can be implemented (33), where T_{ref} is a reference reaction temperature set at 70 °C in this work, T is the actual reaction temperature and A_i is the rate constant at the mean temperature.

$$k_i = A_i \cdot e^{\frac{-E_{a,i}}{R(T-T_{ref})}} \tag{33}$$

Subsequently, the differential equations for the reactants and relevant products can be written (34)-(42). The catalyst bulk density for the reaction is described by ρ.

$$\frac{dc_{Gluc}}{dt} = r_{I,ref} \cdot \rho - r_{II} - r_{IV} \quad (34)$$

$$\frac{dc_{GlucOH}}{dt} = r_{II} - r_{III,ref} \cdot \rho \quad (35)$$

$$\frac{dc_{GlucO}}{dt} = r_{I,ref} \cdot \rho + r_{III,ref} \cdot \rho \quad (36)$$

$$\frac{dc_{Fruc}}{dt} = r_{IV} \quad (37)$$

$$\frac{dc_{Ara}}{dt} = -r_{V,ref} \cdot \rho - r_{VII} \quad (38)$$

$$\frac{dc_{AraL}}{dt} = r_{V,ref} \cdot \rho - r_{VI} \quad (39)$$

$$\frac{dc_{AraOH}}{dt} = r_{VII} - r_{VIII,ref} \cdot \rho \quad (40)$$

$$\frac{dc_{AraO}}{dt} = r_{VI} + r_{VIII,ref} \cdot \rho \quad (41)$$

$$\frac{dc_{Rib}}{dt} = r_{XI} \quad (42)$$

Table 3.9. Simplified reaction model for oxidation of arabinose – glucose mixtures.

Gluc + O_2 ⟶ GlucO
Ara + O_2 ⟶ AraO
Gluc ⟶ Fruc
Ara ⟶ Rib

However, due to the excessive overlapping of peaks during analysis, several components were not possible to quantify. Thus, simplification of the model is necessary where only the most substantial reactions are regarded (Table 3.9). The model is stripped down to only involve the reaction of glucose and arabinose with oxygen to their corresponding aldonic acids, the isomerization of glucose to fructose and the isomerization of arabinose to ribulose. The rate equations are now defined by (43)-(46), where r_1 and r_2 reflect the rates of the oxidation reactions for glucose and arabinose, respectively, and reactions r_1 and r_2 represent the isomerization reactions of glucose and arabinose.

$$r_1 = \frac{k_1 c_{Gluc} c_{O_2}}{\left(1 + K_{Gluc} c_{Gluc} + K_{Ara} c_{Ara} + K_{O_2} c_{O_2}\right)^2} \quad (43)$$

$$r_2 = \frac{k_2 c_{Ara} c_{O_2}}{\left(1 + K_{Gluc} c_{Gluc} + K_{Ara} c_{Ara} + K_{O_2} c_{O_2}\right)^2} \quad (44)$$

$$r_3 = \frac{k_3 c_{Gluc}}{\left(1 + K_{Gluc} c_{Gluc} + K_{Ara} c_{Ara} + K_{O_2} c_{O_2}\right)} \quad (45)$$

$$r_4 = \frac{k_4 c_{Ara}}{\left(1 + K_{Gluc} c_{Gluc} + K_{Ara} c_{Ara} + K_{O_2} c_{O_2}\right)} \quad (46)$$

Since the peaks of arabinose and fructose overlapped during analysis, the concentration of arabinose is described by equation (47),

$$c_{Ara} = c_X - c_{Gluc,0} + c_{Gluc} + c_{GlucO} \tag{47}$$

, where $c_{Gluc,0}$ reflects the initial glucose concentration. Parameter c_X defines the combined concentration of arabinose and fructose. Additionally, the rates are multiplied by the catalyst mass m_{cat} (48)-(51).

$$r_1' = r_1 \cdot m_{cat} \tag{48}$$
$$r_2' = r_2 \cdot m_{cat} \tag{49}$$
$$r_3' = r_3 \cdot m_{cat} \tag{50}$$
$$r_4' = r_4 \cdot m_{cat} \tag{51}$$

Finally, the differential equations for the concentration profiles can be defined (52)-(56), where c_U reflects the concentration of ribulose.

$$\frac{dc_{Gluc}}{dt} = -r_1' - r_3' \tag{52}$$
$$\frac{dc_{GlucO}}{dt} = r_1' \tag{53}$$
$$\frac{dc_X}{dt} = -r_2' - r_4' + r_3' \tag{54}$$
$$\frac{dc_{AraO}}{dt} = r_2' \tag{55}$$
$$\frac{dc_U}{dt} = r_4' \tag{56}$$

As a brief summary, the unknown parameters are defined as the rate constants k_1-k_4, the equilibrium constants K_{Gluc}, K_{Ara} and K_{O_2}, and the activation energies $E_{a,1}$-$E_{a,4}$. The parameter estimation was done by numerically solving the differential equations (52)-(56) with the Simplex method. The best parameter estimation is achieved at the closest correspondence between the estimated fit and the obtained parameters (Fig. 3.22-Fig. 3.24). Thus, the objective function Q is set by maximizing the degree of explanation R^2 (57). The latter is described by the ratio of the squared difference in the experimental (c_{exp}) and the estimated (c_{est}) concentration values, and the square of the differences between c_{exp} and the mean of the estimated concentrations ($\bar{c}_{est}$) [51].

$$Q = \max R^2 = \max 100 \left(\frac{\left(\left\| c_{exp} - c_{est} \right\| \right)^2}{\left(\left\| c_{exp} - \bar{c}_{est} \right\| \right)^2} \right) \tag{57}$$

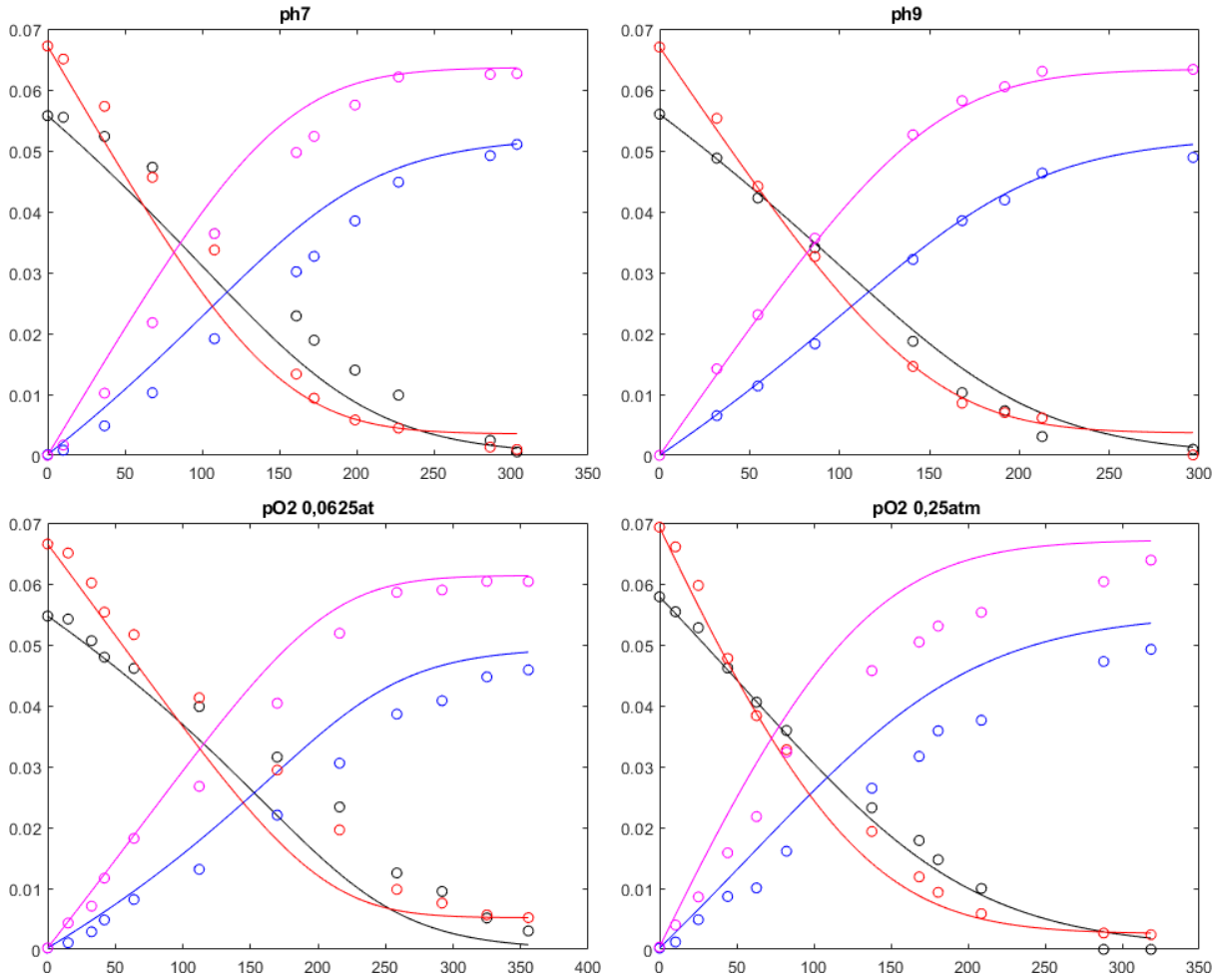

Fig. 3.22. Kinetic model fitted to experimental data from oxidation reactions of 1:1 mass ratio arabinose – glucose mixtures over 1% Au/Al_2O_3-B at (upper row) – different pH and conditions of 70 °C, pO_2 = 0.125 atm and m_{cat} = 0.1 g (down) – different oxygen pressures and conditions of 70 °C, pH 7 and m_{cat} = 0.1 g. vertical axis: concentration [mol/l], horizontal axis: time [min], line: estimated data, circle: experimental data, red: arabinose, black: glucose, pink: arabinonic acid, blue: gluconic acid

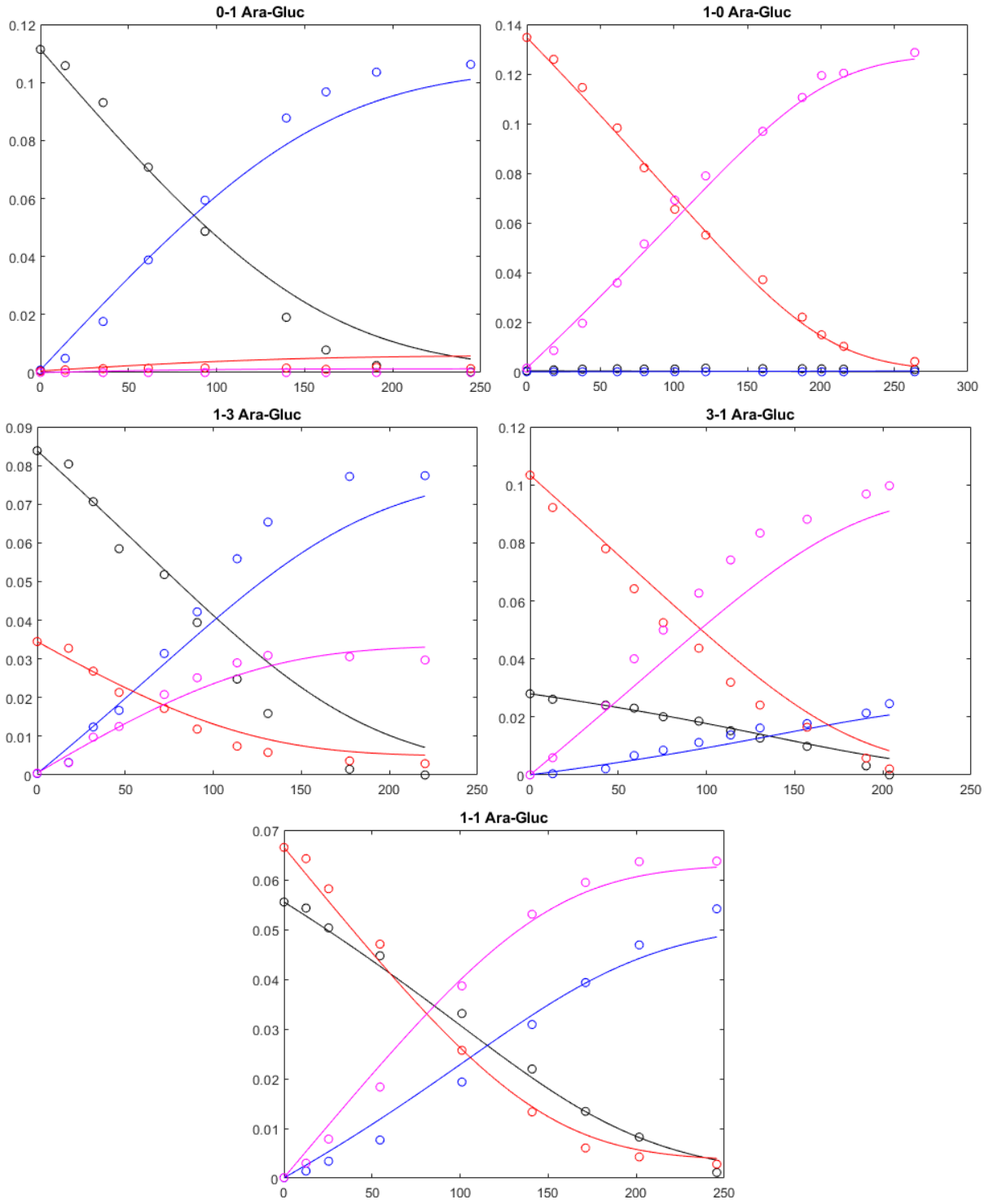

Fig. 3.23. Kinetic model fitted to experimental data from oxidation reactions of arabinose – glucose mixtures with different mass ratios over 1% Au/Al_2O_3-B and conditions of 70 °C, pH 7, pO_2 = 0.125 atm and m_{cat} = 0.1 g. vertical axis: concentration [mol/l], horizontal axis: time [min], line: estimated data, circle: experimental data, red: arabinose, black: glucose, pink: arabinonic acid, blue: gluconic acid

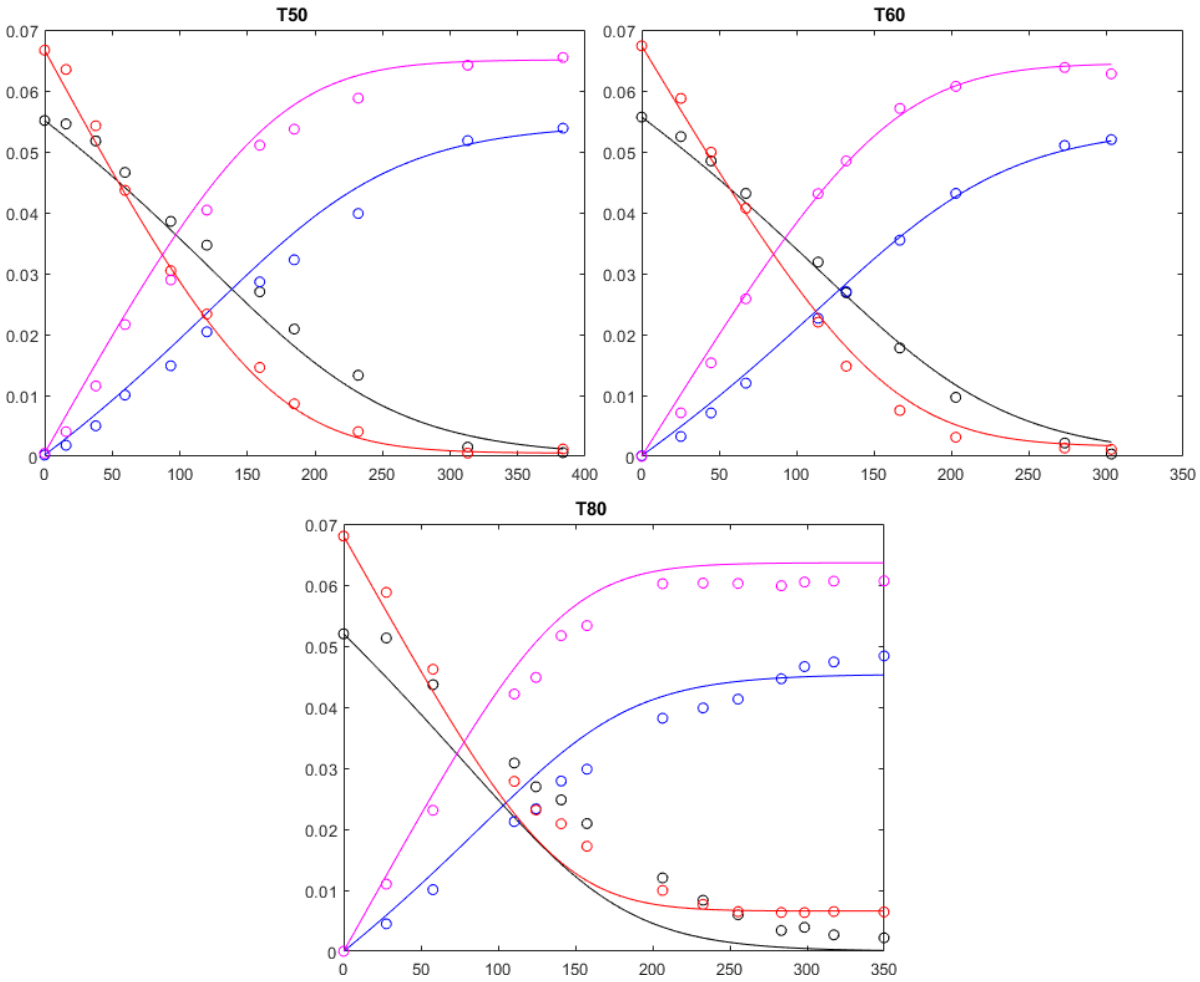

Fig. 3.24. Kinetic model fitted to experimental data from oxidation reactions of 1:1 mass ratio arabinose – glucose mixtures over 1% Au/Al_2O_3-B at different temperatures and conditions pH 7, pO_2 = 0.125 atm and m_{cat} = 0.1 g. vertical axis: concentration [mol/l], horizontal axis: time [min], line: estimated data, circle: experimental data, red: arabinose, black: glucose, pink: arabinonic acid, blue: gluconic acid

The results show that with the values from the parameter estimation are presented in Table 3.10, the simplified model fits the experimental data well with a 97.33% degree of explanation. Although high explanation was confirmed, important to note is that the results display relatively high standard deviations of the parameter values. However, the rate constants for the isomerization processes are minimal compared to the oxidation reactions, allowing to conclude that only minor formations of fructose and ribulose occur in mixtures as well. Important to note is that the experiment with oxygen pressure 0.250 atm was left out during model estimation, as the mass balance closure was inadequate and hence interfering with the other data fitting.

The higher value of the equilibrium constant for arabinose confirms that arabinose adsorption is more favored over glucose. Furthermore, the more significant effect of temperature for arabinose oxidation is also confirmed by the higher activation energy value compared to glucose.

Table 3.10. Results from parameter estimation of the simplified model for oxidation of arabinose – glucose mixtures. k_i – rate constants, K_i – equilibrium constants, $E_{a,i}$ – activation energies

Parameters	Estimated Value	Std. Error	Relative Std. Error (%)	Parameter Std. Error
k_1	0.150E+05	0.343E+04	22.8	4.4
k_2	0.262E+05	0.615E+04	23.5	4.3
k_3	0.250E-01	0.499E-02	19.9	5.0
k_4	0.318E-01	0.671E-02	21.1	4.7
K_{Ara}	0.390E+02	0.558E+01	14.3	7.0
K_{Gluc}	0.206E+02	0.345E+01	16.7	6.0
K_{O2}	0.175E+05	0.259E+04	14.8	6.8
$E_{a,1}$	0.102E+05	0.258E+04	25.2	4.0
$E_{a,2}$	0.583E+04	0.192E+04	33.0	3.0
$E_{a,3}$	0.812E+05	0.216E+05	26.6	3.8
$E_{a,4}$	0.237E+05	0.255E+05	107.4	0.9

Table 3.11 describes how the parameters are correlated to each other, i.e. how one parameter is affected by a change of another parameter value. A high correlation close to 1 indicates that the parameter values are unreliable. In Table 3.11, the highest correlation found is 0.988, while most of the correlations are significantly lower. Hence, the reliability of the estimated parameters can be considered as satisfying.

Table 3.11. Correlation matrix of parameters in Table 3.10.

	k_1	k_2	k_3	k_4	K_{Ara}	K_{Gluc}	K_{O2}	$E_{a,1}$	$E_{a,2}$	$E_{a,3}$	$E_{a,4}$
k_1	1										
k_2	0.988	1									
k_3	0.709	0.732	1								
k_4	0.650	0.677	0.599	1							
K_{Ara}	0.959	0.983	0.740	0.712	1						
K_{Gluc}	0.949	0.934	0.693	0.640	0.933	1					
K_{O2}	0.972	0.966	0.672	0.612	0.908	0.860	1				
$E_{a,1}$	-0.023	-0.060	-0.020	-0.043	-0.064	0.002	-0.058	1			
$E_{a,2}$	-0.113	-0.074	-0.070	-0.024	-0.055	-0.133	-0.101	-0.374	1		
$E_{a,3}$	-0.078	-0.097	-0.458	-0.137	-0.111	-0.087	-0.071	0.020	0.114	1	
$E_{a,4}$	-0.036	-0.036	-0.075	-0.130	-0.044	-0.045	-0.026	-0.153	0.004	0.162	1

4 CONCLUSIONS

Because of the global trend to shift from fossil to bio-based feedstock, the valorization of chemical compounds from biomass is an essential implementation in the concept of biorefining, which oxidation of derived monosaccharides is part of. In this work, aerobic oxidation of arabinose – glucose mixtures over gold nanoparticles in a batch reactor at constant pH has successfully been conducted. A great correlation between catalyst particle size and catalytic activity was observed, giving that catalysts with particles of sizes close to 2-3 nm are favored for aldose oxidation reactions. High $\overline{d_p}$ for carbon-supported catalysts resulted in low or no activity. Consequently, catalysts supported on Al_2O_3 showing significantly lower d_p are more suitable for oxidation reactions.

Oxidation reactions of arabinose – glucose mixtures over 1% Au/Al_2O_3-B revealed that oxidation of arabinose (C5) is more favored compared to glucose (C6) under all conditions investigated. Computed results confirmed a more favored adsorption of arabinose. Furthermore, studies of mutarotational processes show a higher content of reactive components for arabinose under investigated conditions.

Due to mutarotation, the highest productivity is obtained with arabinose – glucose mixtures with 3:1 mass ratio (0.78:0.22 molar ratio). From aldose-to-gold molar ratios of 24200:1 and above, the rate is not limited by mass transfer processes. Furthermore, arabinose oxidation shows higher influence by catalyst loading. Oxidation reactions of arabinose – glucose mixtures with 1:1 mass ratio (0.55:0.45 molar ratio) under varying conditions of temperature, pH and oxygen pressure, rate maxima were achieved at 70 °C, pH 8 and 0.125 atm. For arabinose, the results at 60 °C and 70 °C were identical while for glucose, the results were identical for oxygen pressure 0.125 atm and 0.250 atm. At these conditions, the reaction order of both arabinose and glucose oxidation was close to 0^{th} order. For deeper understanding of the influence of oxygen pressure, further experiments have to be conducted.

Overall, high selectivity to the corresponding aldonic acids was achieved under all conditions. These highest selectivity of almost 100% to both arabinonic acid and gluconic acid, respectively, was achieved at the above-mentioned conditions, i.e. 70 °C, pH 8 and 0.125 atm oxygen pressure, thus making them most suitable for the reaction. Temperatures over 70 °C induce catalyst deactivation and pH values above 8 enhance the formation of by-products, especially for glucose. Thus, for optimal selectivity, only a narrow condition interval is

available. Further investigations showed that catalyst deactivation after washing process prohibits recycling of the catalyst.

Due to analytical issues, a simplified model had to be derived with only the main reactions and isomerization processes, thus excluding any intermediate steps. The model was confirmed to fit the experimental data well with an R^2 of 97.33%.

SWEDISH SUMMARY – SVENSK SAMMANFATTNING

Under de senaste årtiondena har till följd av klimatförändringen och minskade tillgångar trenden att frångå fossila bränslen och råmaterial ökat massivt. Konceptet för utnyttjandet av biomassa för att ersätta fossila motsvarande har blivit av stort intresse och forskning inom området är högaktuell. Idag används biomassa främst för att framställa energi genom förbränning. För utnyttjandet av biomassans kemiska innehåll och egenskaper finns alternativa metoder som pyrolys, förgasning, extraktion och hydrolys.

Lignocellulosa, dvs. torr biomassa, består av tre delar: cellulosa, hemicellulosa och lignin. De två förstnämnda består av sackarider. Cellulosa innehåller endast polymerkedjor av glukos som består av sex kolatomer (C6), medan hemicellulosa är ett samlingsnamn och kan bestå av olika länkade monosackarider med både fem (C5) och sex (C6) kolatomer. Arabinogalaktan har exempelvis en ryggrad av β-D-galaktos med förgreningar av β-D-galaktos, α-L-arabinos och glukonsyra. Genom hydrolys fraktioneras polysackariderna i biomassan till monosackarider. Dessa monosackarider utgör en bas för vidare kemikalieframställning ur biomassa. Hydrering av aldoser (glukos, arabinos, galaktos) ger motsvarande alditoler och vice versa resulterar oxidering i bildningen av syror, endera aldonsyror, uronsyror eller aldariska syror (eng. *aldonic acids, uronic acids, aldaric acids*). Dessa syror används i bland annat matprodukter, kosmetika och läkemedelsprodukter.

Framförallt den katalytiska oxideringen av glukos har tidigare studerats intensivt. Utöver det visade Kusema et al. hydreringen av arabinogalaktan samt separat oxidering av arabinos och galaktos. Ytterligare publicerades studier om hydrering av sockerblandningar i arbetet av Herrera et al. Inga studier om oxideringen av sockerblandningar har dock publicerats, vilket görs i det här arbetet.

Oxideringen av glukos (C6) har i tidigare studier rapporterats genom både heterogena och enzymatiska katalytiska processer. Enzymer uppvisar dock nackdelar när det kommer till förvaring och användningsförhållanden. I litteratur om oxidering av arabinos (C5) har tidigare alltid använts heterogena katalysatorer som bland annat platina, palladium och guld. Nackdelen med de två förstnämnda har dock konstaterats vara överoxidering av metallen, vilket leder till att katalysatorn inaktiveras. Guld har bevisats att undgå detta fenomen och är fördelaktigt för oxideringsreaktioner, varför det använts i det här arbetet.

I vattenlösningar uppträder både glukos och arabinos i olika former: en öppen form och fyra ringstrukturer, α-och β-pyranos samt α- och β-furanos. Pyranos är i majoritet medan den öppna formen och furanosformerna uppträder i endast marginella mängder och är mera instabila komponenter. De instabila egenskaperna antyder att det är den öppna och furanosformerna som är de aktiva komponenterna i reaktionen. Därav uppstår två oxidationsreaktionsrutter för vardera sackariden. Den ena rutten går över den ringformade furanosstrukturen som adsorberas vid katalysatorn och oxideras till aldonens lakton. Efter desorption från katalysatorn inducerar den basiska miljön öppningen av ringstrukturen och aldonsyra erhålls, som i basisk miljö dehydreras till glukonat. Den andra rutten förlöper över den öppna formen, som i basisk miljö katalyseras till aldehydrol. Denna adsorberas på katalysatorn, oxideras till glukonsyra och desorberas. Igen övergår glukonsyra till glukonat i det basiska mediet.

För att studera den aerobiska oxideringen av blandningar med glukos och arabinos undersöktes sex parametrar: inverkan av katalysatorbärare, arabinos- och glukoskoncentrationsförhållanden, temperatur, pH, partialtrycket av syre samt massan katalysator i reaktionen. Katalysatorns stabilitet undersöktes även till viss mån. Slutligen utvecklades en kinetisk modell för att matematiskt beskriva reaktionerna. Samtliga experiment utfördes i en satsreaktor med hög omrörningshastighet vid atmosfärstryck samt under kontrollerade temperatur- och pH-förhållanden. pH justerades med tillsatt NaOH. Den totala sockerkoncentrationen hölls vid 20 g/l. Syrgas tillsattes tillsammans med argon, vilken fungerade som inert.

Skillnaderna i katalysatorbärare framgår främst ur den aktiva metallens partikelstorlek på katalysatorn. Inverkan av partikelstorleken är av stor vikt eftersom oxideringsreaktioner har visats vara starkt påverkade av den. Katalysatorns aktivitet är beroende av temperatur och pH, samtidigt som pH även inverkar på produkterna. Eftersom syre behövs för oxidering var reaktionen beroende av tillgången till syre samt ledig katalysator, som påverkades av mängden katalysator i reaktionen.

Resultaten visar att oxideringen av arabinos var klart effektivare än glukosoxidering i samtliga sammanhang. Guldpartikelstorleken på de analyserade kolbaserade katalysatorbärarna (både 1 viktprocent och 2 viktprocent Au) var klart högre än för Al_2O_3-katalysatorbärare med 1 viktprocent Au. Oxideringsreaktioner under identiska förhållanden visade jämförbara resultat med mycket högre reaktionshastigheter för Au/Al_2O_3-katalysatorer. Den mest aktiva katalysatorn visade en partikelstorleksfördelning för partiklar $\leq$ 10 nm på 2,63 nm. Denna katalysator användes för samtliga fortsatta parameterundersökningar i studien. Beträffande

reaktionshastigheter samt selektivitet uppvisades den optimala temperaturen ligga vid 70 °C tillsammans med pH 8 och pO_2 = 0,125 atm. Högre pH-värden orsakade försämrad selektivitet för aldonsyrorna. Utöver detta uppvisade förhöjda temperaturer långsammare reaktionshastigheter. Reaktionshastigheterna visades vara direkt korrelerade till sockerkoncentrationerna vid lägre halter, ökande med förhöjt koncentrationsförhållande. Däremot stagnerade reaktionshastigheterna från och med förhållanden från 0,75 för vardera monosackariden. Den mest effektiva katalysatormängden i en reaktion konstaterades till 0,1 g av den mest aktiva 1% Au/Al_2O_3-katalysatorn. Dock visade recirkulering av katalysatorn inaktivering av denna under de givna förhållandena.

Den kinetiska modellen konstruerades enligt reaktionsmekanismerna och koncentrationsprofilernas differentialekvationer definierades. Genom numerisk parameterestimering anpassades modellen med dess koncentrationsekvation till de experimentella data.

REFERENCES

[1] CH-Bioforce, "CH-Bioforce - Technology," 2019. [Online]. Available: https://www.ch-bioforce.com/technology/.

[2] D. Y. Murzin and I. L. Simakova, "Catalysis in Biomass Processing," in *Comprehensive Inorganic Chemistry II (Second Edition): From Elements to Applications*, 2013.

[3] A. Sundberg, "PCC Biorefinery Building Blocks of Biomass," 2015.

[4] P. M. Collins and R. J. Ferrier, *Monosaccharides : their chemistry and their roles in natural products*. Wiley, 1995.

[5] L. P. S. Vandenberghe, S. G. Karp, P. Z. de Oliveira, J. C. de Carvalho, C. Rodrigues, and C. R. Soccol, "Solid-State Fermentation for the Production of Organic Acids," in *Current Developments in Biotechnology and Bioengineering*, 2018.

[6] S. Guo, Q. Fang, Z. Li, J. Zhang, J. Zhang, and G. Li, "Efficient base-free direct oxidation of glucose to gluconic acid over TiO 2 -supported gold clusters," *Nanoscale*, 2019.

[7] R. Wojcieszak, I. M. Cuccovia, M. A. Silva, and L. M. Rossi, "Selective oxidation of glucose to glucuronic acid by cesium-promoted gold nanoparticle catalyst," *J. Mol. Catal. A Chem.*, 2016.

[8] E. Derrien, M. Mounguengui-Diallo, N. Perret, P. Marion, C. Pinel, and M. Besson, "Aerobic Oxidation of Glucose to Glucaric Acid under Alkaline-Free Conditions: Au-Based Bimetallic Catalysts and the Effect of Residues in a Hemicellulose Hydrolysate," *Ind. Eng. Chem. Res.*, 2017.

[9] B. T. Kusema *et al.*, "Kinetics of acid hydrolysis of arabinogalactans," *Int. J. Chem. React. Eng.*, 2010.

[10] E. Smolentseva *et al.*, "Selective oxidation of arabinose to arabinonic acid over Pd-Au catalysts supported on alumina and ceria," *Appl. Catal. A Gen.*, 2011.

[11] B. T. Kusema *et al.*, "Selective Oxidation of D-Galactose over Gold Catalysts," *ChemCatChem*, 2011.

[12] V. A. S. Herrera, F. Saleem, B. Kusema, K. Eränen, and T. Salmi, "Hydrogenation of L-arabinose and D-galactose mixtures over a heterogeneous Ru/C catalyst," in *Topics in Catalysis*, 2012.

[13] L. S. Correia, H. Grénman, J. Wärnå, T. Salmi, and D. Y. Murzin, "Catalytic oxidation kinetics of arabinose on supported gold nanoparticles," *Chem. Eng. J.*, vol. 370, no. December 2018, pp. 952–961, 2019.

[14] G. J. Hutchings, "Catalysis by gold," in *Catalysis Today*, 2005.

[15] M. Haruta, T. Kobayashi, H. Sano, and N. Yamada, “ChemInform Abstract: Novel Gold Catalysts for the Oxidation of Carbon Monoxide at a Temperature Far Below 0°C.,” *ChemInform*, 1987.

[16] A. Corma and H. Garcia, “Supported gold nanoparticles as catalysts for organic reactions,” *Chemical Society Reviews*. 2008.

[17] M. Besson, F. Lahmer, P. Gallezot, patrick Fuertes, and G. Fleche, “Catalytic oxidation of glucose on bismuth-promoted palladium catalysts,” *J. Catal.*, 1995.

[18] P. J. M. Dijkgraaf, M. J. M. Rijk, J. Meuldijk, and K. van der Wiele, “Deactivation of platinum catalysts by oxygen. 1. Kinetics of the catalyst deactivation,” *J. Catal.*, 1988.

[19] V. R. Gangwal, J. Van Der Schaaf, B. F. M. Kuster, and J. C. Schouten, “Influence of pH on noble metal catalysed alcohol oxidation: Reaction kinetics and modelling,” *J. Catal.*, 2005.

[20] A. V. Tokarev, E. V. Murzina, J. P. Mikkola, J. Kuusisto, L. M. Kustov, and D. Y. Murzin, “Application of in situ catalyst potential measurements for estimation of reaction performance: Lactose oxidation over Au and Pd catalysts,” *Chem. Eng. J.*, 2007.

[21] B. T. Kusema, B. C. Campo, P. Mäki-Arvela, T. Salmi, and D. Y. Murzin, “Selective catalytic oxidation of arabinose - A comparison of gold and palladium catalysts,” *Appl. Catal. A Gen.*, 2010.

[22] I. V. Delidovich *et al.*, “Aerobic selective oxidation of glucose to gluconate catalyzed by Au/Al2O3 and Au/C: Impact of the mass-transfer processes on the overall kinetics,” *Chem. Eng. J.*, 2013.

[23] L. Prati, A. Villa, A. R. Lupini, and G. M. Veith, “Gold on carbon: One billion catalysts under a single label,” *Physical Chemistry Chemical Physics*. 2012.

[24] C. Megías-Sayago *et al.*, “Influence of gold particle size in Au/C catalysts for base-free oxidation of glucose,” *Catal. Today*, 2018.

[25] C. Liu *et al.*, “Efficient Aerobic Oxidation of Glucose to Gluconic Acid over Activated Carbon-Supported Gold Clusters,” *ChemSusChem*, 2017.

[26] J. M. Hornback, *Organic Chemistry*. 2006.

[27] J. F. Lopes and E. M. S. M. Gaspar, “Simultaneous chromatographic separation of enantiomers, anomers and structural isomers of some biologically relevant monosaccharides,” *J. Chromatogr. A*, 2008.

[28] M. Wu *et al.*, “Isomeric distribution of monosaccharides in deep eutectic solvents: NMR study,” *J. Mol. Liq.*, 2018.

[29] M. L. Sinnott, *Carbohydrate Chemistry and Biochemistry: Structure and Mechanism*.

2007.

[30] R. O. L. Souza, D. P. Fabiano, C. Feche, F. Rataboul, D. Cardoso, and N. Essayem, “Glucose-fructose isomerisation promoted by basic hybrid catalysts,” *Catal. Today*, 2012.

[31] R. S. Tipson and D. Horton, *Advances in Carbohydrate Chemistry and Biochemistry*. 1984.

[32] P. Langan *et al.*, “L-Arabinose binding, isomerization, and epimerization by D-Xylose isomerase: X-Ray/Neutron crystallographic and molecular simulation study,” *Structure*, 2014.

[33] W. Xu, W. Zhang, T. Zhang, B. Jiang, and W. Mu, “L-arabinose isomerases: Characteristics, modification, and application,” *Trends in Food Science and Technology*. 2018.

[34] D. Y. Murzin *et al.*, “Aldose to ketose interconversion: Galactose and arabinose isomerization over heterogeneous catalysts,” *Catal. Sci. Technol.*, 2017.

[35] N. M. Deraz, “The comparative jurisprudence of catalysts preparation methods: II. Deposition-precipitation and adsorption methods.,” *J Ind Env. Chem*, vol. 2, no. 2, pp. 1–3, 2018.

[36] S. Ivanova, V. Pitchon, Y. Zimmermann, and C. Petit, “Preparation of alumina supported gold catalysts: Influence of washing procedures, mechanism of particles size growth,” *Appl. Catal. A Gen.*, 2006.

[37] O. A. Simakova *et al.*, “Structure sensitivity in L-arabinose oxidation over Au/Al2O 3 catalysts,” *J. Phys. Chem. C*, vol. 115, no. 4, pp. 1036–1043, 2011.

[38] Y. C. Zhao, D. L. Yu, H. W. Zhou, Y. J. Tian, and O. Yanagisawa, “Turbostratic carbon nitride prepared by pyrolysis of melamine,” in *Journal of Materials Science*, 2005.

[39] R. Zanella, S. Giorgio, C. R. Henry, and C. Louis, “Alternative methods for the preparation of gold nanoparticles supported on TiO2,” *J. Phys. Chem. B*, 2002.

[40] E. V. Murzina, A. V. Tokarev, K. Kordás, H. Karhu, J. P. Mikkola, and D. Y. Murzin, “d-Lactose oxidation over gold catalysts,” *Catal. Today*, 2008.

[41] “ImageJ.” 2016.

[42] A. H. Munhoz, H. de Paiva, L. F. de Miranda, E. C. De Oliveira, R. Cons Andrades, and A. C. Neto, “Synthesis and characterization of pseudoboehmite and gamma-alumina,” in *Materials Science Forum*, 2015.

[43] O. Corporation, “Origin.” Northampton, MA, USA, 2019.

[44] D. Tromans, “Temperature and pressure dependent solubility of oxygen in water: A

thermodynamic analysis," *Hydrometallurgy*, 1998.

[45] T. Ishida, N. Kinoshita, H. Okatsu, T. Akita, T. Takei, and M. Haruta, "Influence of the support and the size of gold clusters on catalytic activity for glucose oxidation," *Angew. Chemie - Int. Ed.*, 2008.

[46] B. T. Kusema and D. Y. Murzin, "Catalytic oxidation of rare sugars over gold catalysts," *Catalysis Science and Technology*. 2013.

[47] P. Pal, R. Kumar, and S. Banerjee, "Manufacture of gluconic acid: A review towards process intensification for green production," *Chemical Engineering and Processing: Process Intensification*. 2016.

[48] S. Biella, L. Prati, and M. Rossi, "Selective oxidation of D-glucose on gold catalyst," *J. Catal.*, 2002.

[49] B. T. Kusema, J. P. Mikkola, and D. Y. Murzin, "Kinetics of L-arabinose oxidation over supported gold catalysts with in situ catalyst electrical potential measurements," *Catal. Sci. Technol.*, 2012.

[50] J. M. Gottfried, K. J. Schmidt, S. L. M. Schroeder, and K. Christmann, "Spontaneous and electron-induced adsorption of oxygen on Au(1 1 0)-(1 × 2)," *Surf. Sci.*, 2002.

[51] H. Haario, "Modest User's Guide," Helsinki, 1994.

APPENDICES

Appendix I

HPLC – RI calibration data and results

Table Appendix - 1. Data from HPLC-IR calibration.

0,6 ml/min		RSQ	SLOPE	INTERCEPT			RSQ	SLOPE	INTERCEPT
g/100ml	Area				g/100ml	Area			
Arabinose		0.999	1.045E-07	-0.0075	**Glucose**		0.998	9.983E-08	-0.0118
1.001	9538167				1.001	9985368			
0.5005	5083945				0.5005	5424184			
0.25025	2498199				0.25025	2663970			
0.125125	1241156				0.125125	1344712			
0.0625625	626937				0.062563	686336			
0.0312813	309413				0.031281	342045			
D-Arabinonic acid		1.000	7.765E-08	0.0176	**Gluconic acid**		0.997	8.151E-08	-0.0314
0.960	12112014				2.070	25644730			
0.480	6168451				1.035	12800747			
0.240	2986419				0.518	7774024			
0.120	1347142				0.259	3457447			
0.060	612389				0.129	1723761			
0.030	132077				0.065	905343			
D-Arabino-γ-lactone		0.993	8.787E-08	-0.0057	**Glucuronic acid**		1.000	7.001E-08	0.0288
0.1	1222032				1	13790500			
0.05	594042.6				0.5	6895075			
0.025	313076.1				0.25	3188202			
0.0125	221771.3				0.125	1300779			
0.00625	175473.7				0.0625	440074			
Ribulose		N/A	N/A	N/A	**Fructose**		1.000	9.856E-08	0.0048
~1,35	24450213				0.5	5017173			
					0.25	2509506			
					0.125	1202803			
					0.0625	587311			

0,3 ml/min		RSQ	SLOPE	INTERCEPT			RSQ	SLOPE	INTERCEPT
g/100ml	Area				g/100ml	Area			
Arabinose		1.000	4.976E-08	7.019E-04	**Glucose**		1.000	5.023E-08	8.868E-03
2.004	40244811				1.950	38701425			
1.002	20172082				0.975	19150410			
0.501	9981169				0.488	9418298			
0.250	5029364				0.244	4655132			
0.125	2524018				0.122	2401375			
Arabinonic acid		1.000	4.085E-08	-8.150E-03	**Glucuronic acid**		1.000	3.492E-08	1.676E-02
1.022	25082561				1.503	4.23E+07			
0.511	12843098				0.752	2.15E+07			
0.256	6705398				0.376	1.02E+07			
0.128	3364105				0.188	5.34E+06			
0.064	1730309				0.094	2.11E+06			
0.032	720461				0.047	4.38E+05			
Arabino-y-lactone		0.984	3.600E-08	-2.743E-02	**Gluconic acid**		1.000	4.045E-08	8.558E-03
1.273	34877362				2.070	50980900			
0.636	20334333				1.035	25382821			
0.318	10607999				0.518	12553103			
0.159	3524434				0.259	5990904			
					0.129	3074750			
					0.065	1498057			

Appendix II

Catalyst particle size distributions.

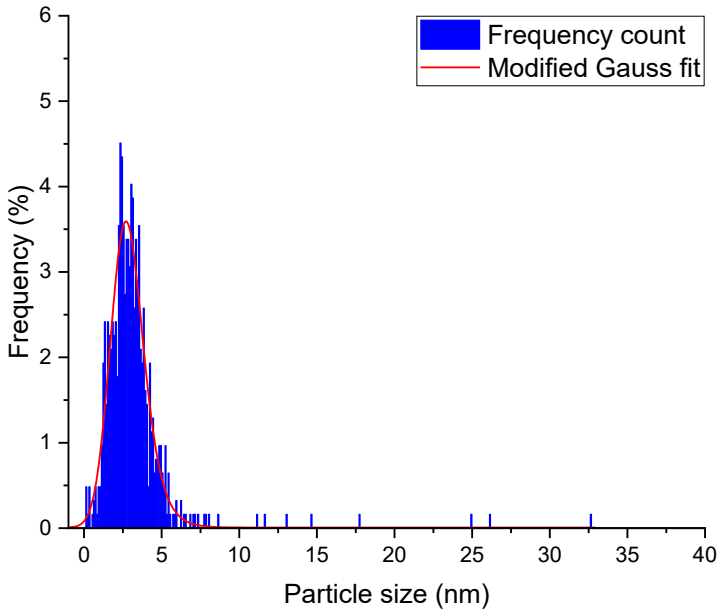

Fig. Appendix - 1. PSD for 1% Au/Al_2O_3-A.

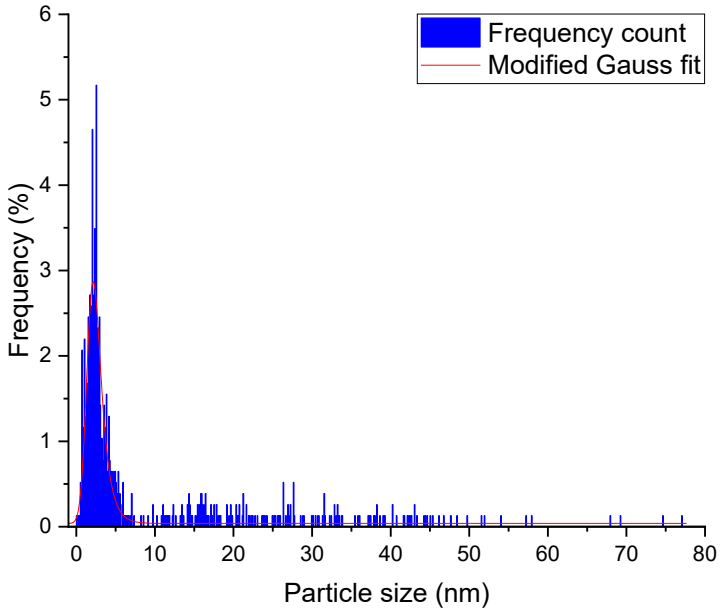

Fig. Appendix - 2. PSD for 1% Au/Al_2O_3-B.

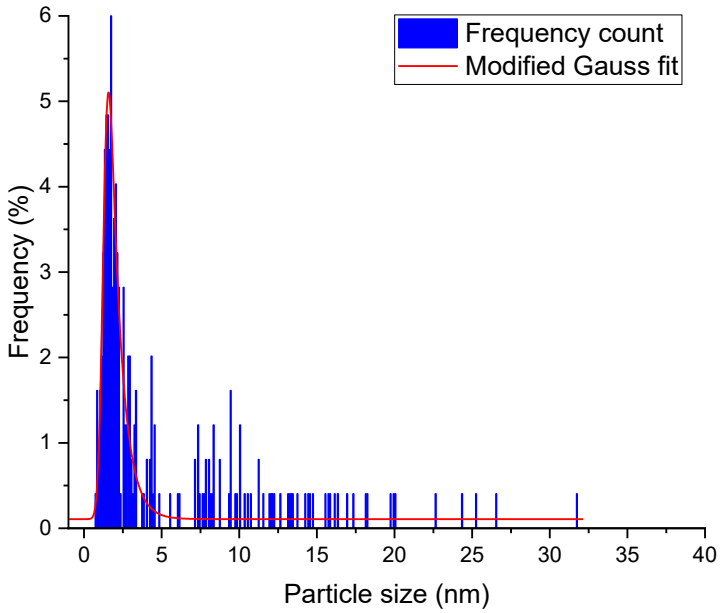

Fig. Appendix - 3. PSD for 1% Au/Al_2O_3 –C.

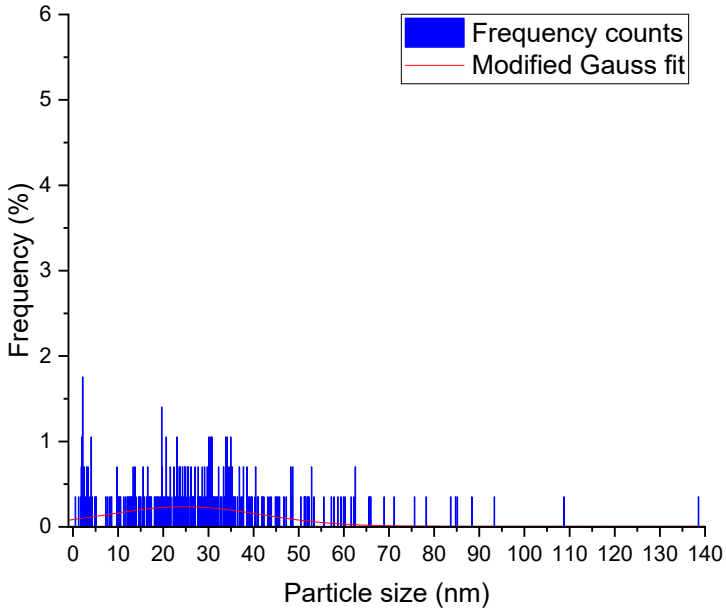

Fig. Appendix - 4. PSD for 2% Au/C-MCF.

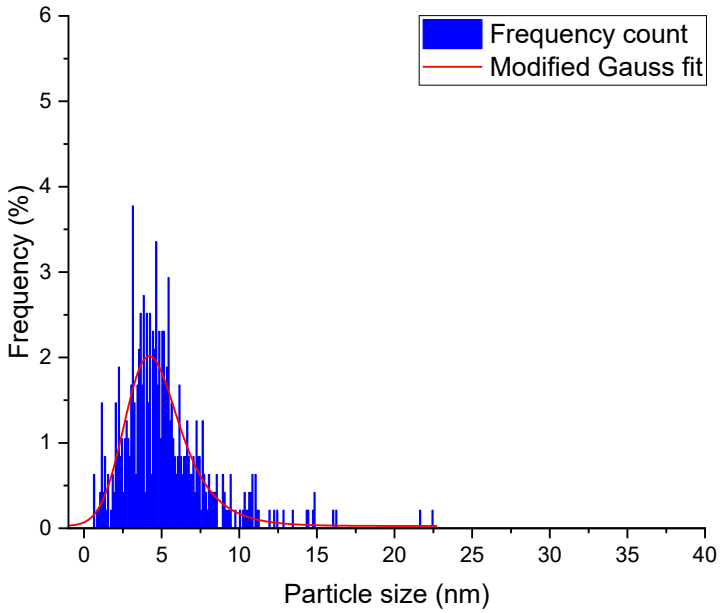

Fig. Appendix - 5. PSD for 1% Au/C.

Appendix III

Results from oxidation reactions of arabinose – glucose mixture with varying mass ratios over 1% Au/Al_2O_3-B and conditions of 70 °C, pH 8 and pO_2 = 0.125 atm.

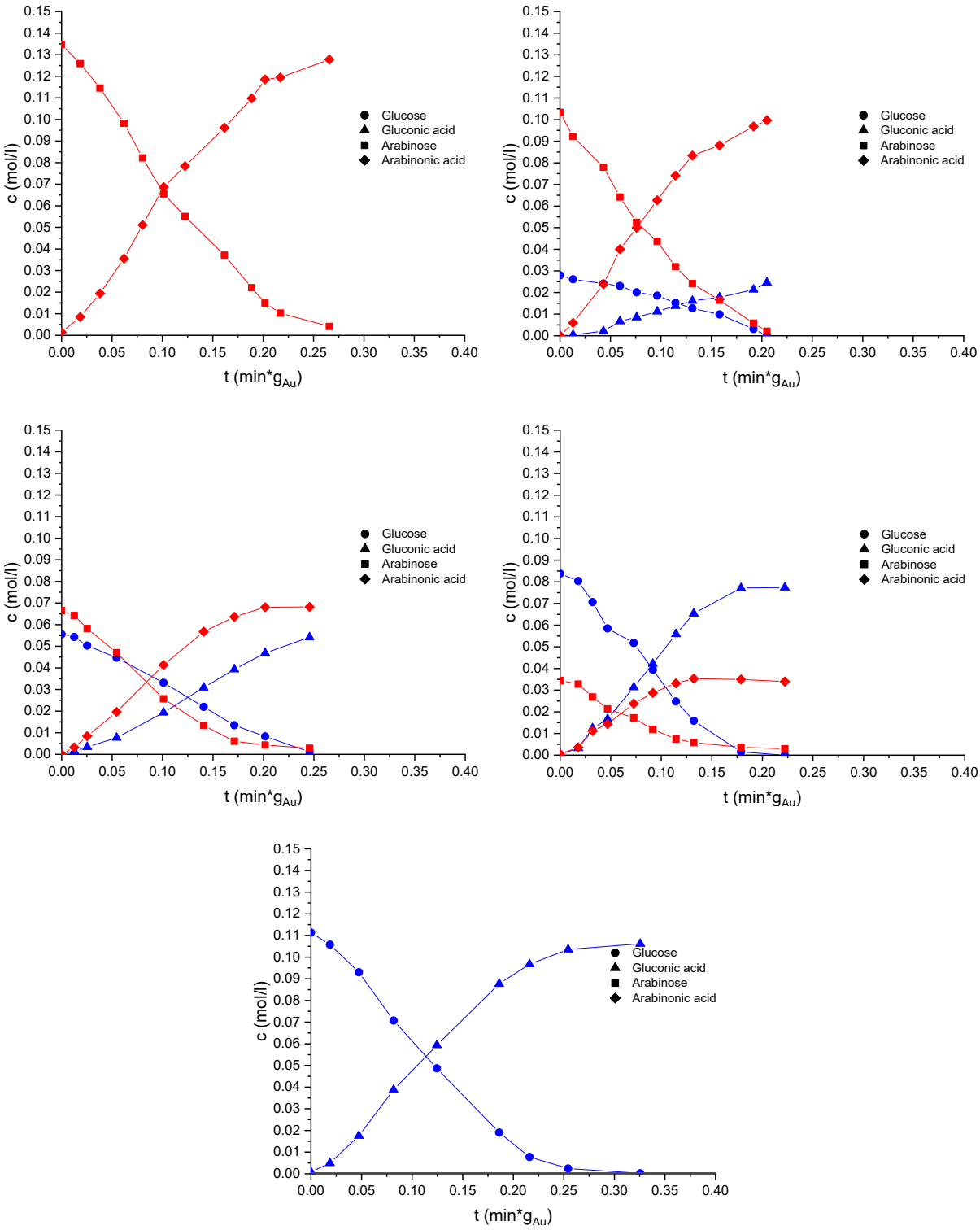

Fig. Appendix - 6. Oxidation reactions of arabinose – glucose mixtures with different mass ratios over 1% Au/Al_2O_3-B. Up-left - 1:0, up-right - 075:0.35, mid-left – 0.5:0.5, mid-right – 0.25:0.75, down – 0:1.

Appendix IV

HPLC of individual sugar reactions

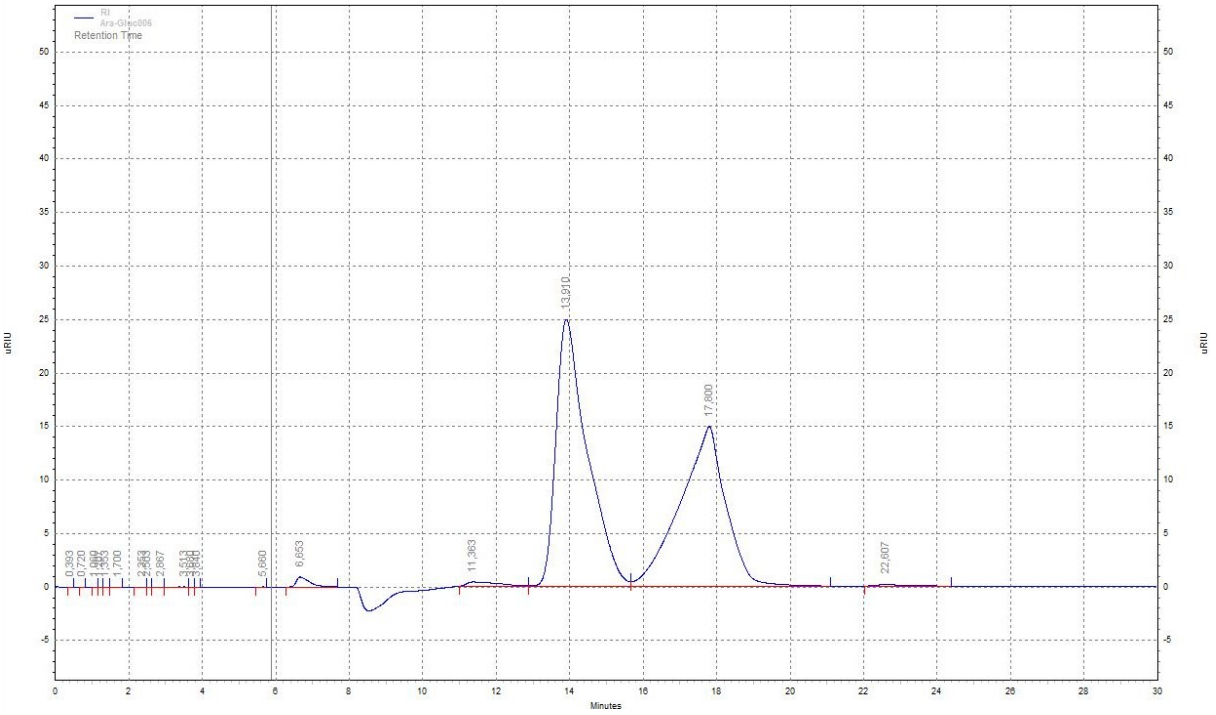

Fig. Appendix - 7. HPLC graph of arabinose oxidation at t = 80 min. Retention times: 6.7 min – Unknown product, 11.4 min – Arabinolactone, 13.9 min – Arabinose, 17.8 min – Arabinonic acid, 22.6 min – Ribulose.

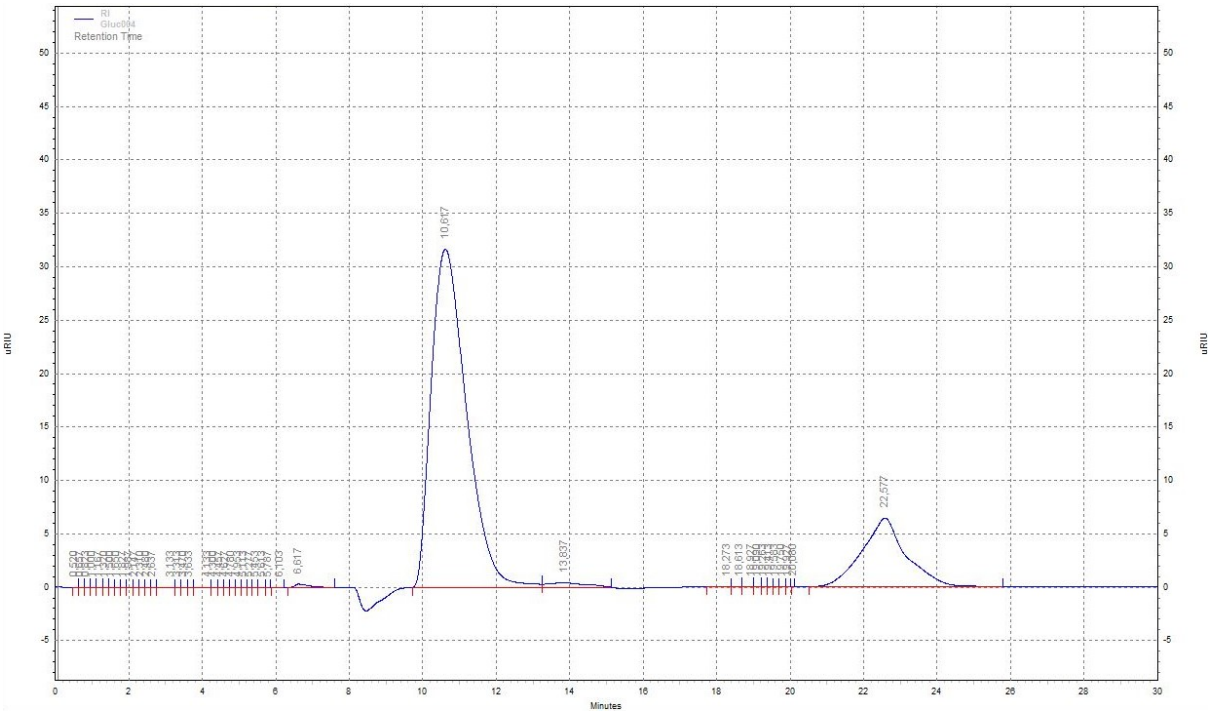

Fig. Appendix - 8. HPLC graph of glucose oxidation at t = 60 min. Retention times: 6.2 min – Unknown product, 10.6 min – Glucose, 13.8 min – Fructose, 22.6 min – Gluconic acid.

Appendix V

Results from oxidation reactions of arabinose – glucose mixtures with 1:1 mass ratio at different temperatures over 1% Au/Al_2O_3-B and conditions of pH 8, pO_2 = 0.125 atm and m_{cat} = 0.1 g.

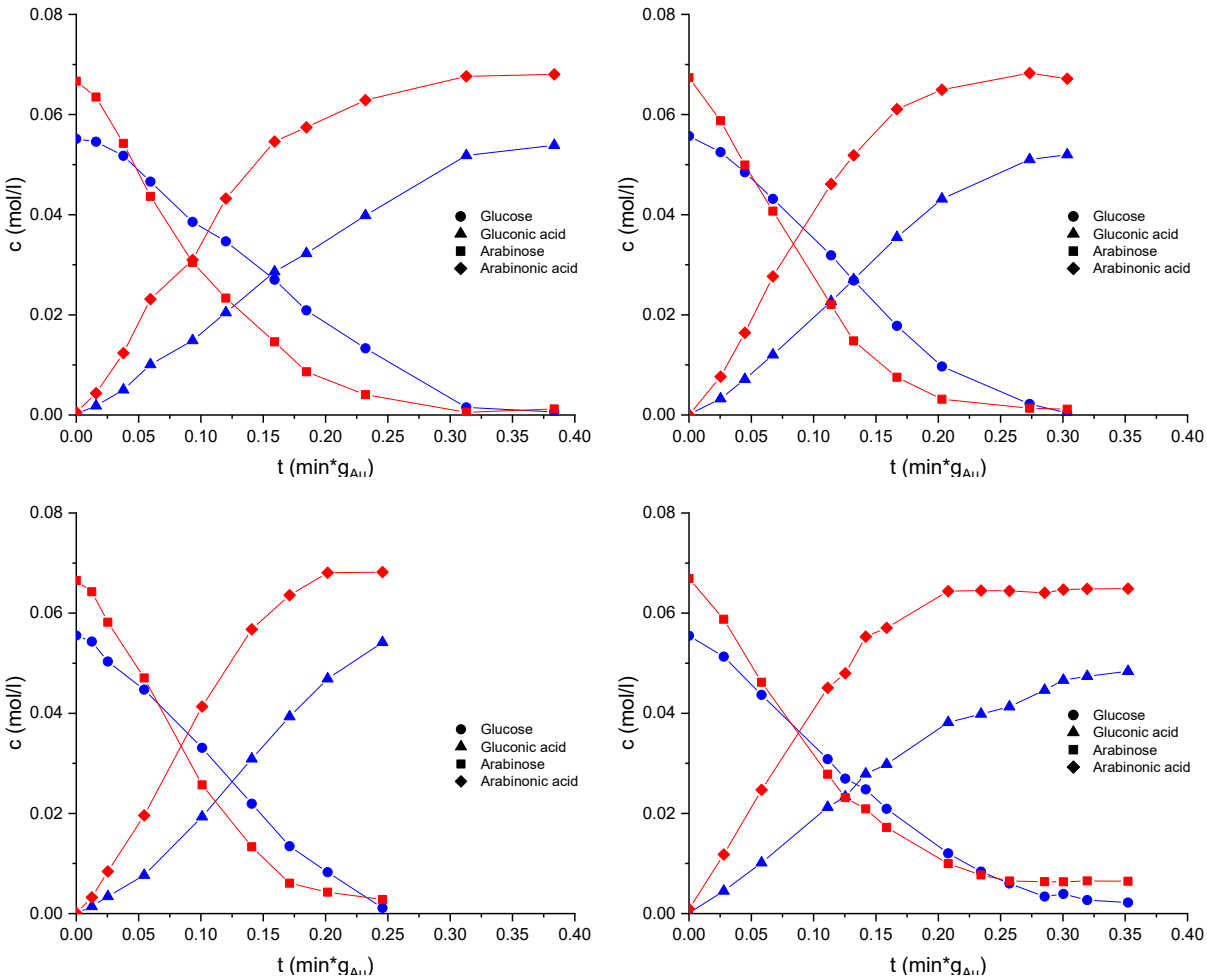

Fig. Appendix - 9. Oxidation reactions of arabinose – glucose mixtures over 1% Au/Al_2O_3-B at varying temperatures.

Appendix VI

ICP – MS results for spent 1% Au/Al_2O_3-B catalyst.

Table Appendix - 2. ICP-MS results for liquid phase sample from arabinose – glucose oxidation over 1% Au/Al_2O_3-B. Sample was taken at the end of the reaction.

Sample mass	Element	M_{Au}	c	SD	RSD
g		g/mol	µg/kg	µg/kg	%
0.5	Au	197	15	2.5	16.8